International Journal of Fatigue 178 (2024) 107996

Contents lists available at ScienceDirect

International Journal of Fatigue

journal homepage: www.elsevier.com/locate/ijfatigue

Misalignment factors to affect the fatigue of welded load-carrying joints

Marco Soligo [a], Alberto Campagnolo [a], Giovanni Meneghetti [a], Halid Can Yıldırım [b,*]

[a] Department of Industrial Engineering, University of Padova, Padova, 35131, Italy
[b] Department of Civil and Architectural Engineering, Aarhus University, Aarhus, 8000, Denmark

ARTICLE INFO

Keywords:
Weld fatigue
Steel
Misalignment
Local stress assessment

ABSTRACT

To assess the effects of misalignment on the weld fatigue, we present experimental fatigue test results of load-carrying cruciform joints which are subjected to axial variable amplitude loading. The welds were produced from steel AH36 grade and fatigue strength improved by high-frequently mechanical impact treatment. We identify several misalignment factors affecting the fatigue by considering the real and reference welded joint geometries. Our methodology includes proposals for the empirical calibration functions and local stress analyses by using the Structural Hot Spot Stress, Effective Notch Stress and Peak Stress Method. Additionally, we apply our methodology to other sixteen data sets which are extracted from the literature for load-carrying cruciform and butt welded joints subjected to constant amplitude loading. Finally, we present the resultant calibration functions with respect to corresponding fatigue test data.

1. Introduction

Steel is the major material in the production development, e.g., in construction equipment, infrastructures, energy sector, oil and gas industry as well as transportation. Under cyclic loading, welds are usually the most critical regions because of the poor fatigue performance due to welding process. In some cases, the better fatigue performance can be realised by employing good, detailed design practices, for example by locating welds in low-stressed regions, but this is not practical in most applications. Alternatively, one can add extra plates or components to redistribute the service stresses close to the weld area. However, this is usually limited since it leads to an increase in the total weight of the component and the cost involved. A more sustainable way is to utilise a higher steel grades to satisfy the strength requirements with a smaller plate thickness, which brings two main challenges. The first limitation is the fact that the fatigue properties at the weld are only equivalent to those of low strength steel grades. The second one is the misalignments as the plate thickness gets smaller. This is even more critical issue when the weld is a load carrying component.

The misalignment in welded structures is due to the thermal-input during welding resulting with the mechanical restraints. In many cases the misalignment effect cannot be completely avoided because they have an influence on the fatigue life of the welded joints. The main cause for the reduction in fatigue strength of misaligned welded joints is thought to be the introduction of additional tensile stress due to the presence of a secondary bending. These effect also increase the degree of stress and strain concentration, which deteriorates the fatigue properties of the welded joints. Even though an acceptable misalignment is allowed based on the use cases, there is a need to understand and quantify the affecting factors on the weld fatigue.

A variety of local fatigue assessment procedures for welded structures has been developed, considering both analytical and numerical methods. A comprehensive survey of these methods can be found in Radaj et al. [1], mainly for analytical solutions. On the other hand, relevant numerical assessments were proposed based on the use of finite element (FE) methods, which can take into account of weld detail and loading conditions (such as Constant or Variable Amplitude Loading), geometric parameters, fracture properties and welding defects. Thus far, the IIW has developed and published detailed guidelines concerning two local fatigue design approaches for welded components: the SHSS method [2] and the ENS method [3]. Besides these local methods, the intensity at the notches have also been widely studied. These include but not limited to Notch Stress Intensity Factors (NSIF) [4] and Strain Energy Density (SED) [5], which have an good potential for further applications of weld fatigue. Furthermore, a more recently developed Peak Stress Method (PSM) allows to determine the value of NSIFs rapidly to assess the weld fatigue by using courses meshes obtained in FE models.

One of the first best-practice recommendations on the post-weld treatment (PWT) methods for steel and aluminium structures were published by ihe International Institute of Welding (IIW) [6]. The guideline included four traditional PWT methods: burr-grinding, tungsten inert gas (TIG) re-melting, hammer peening, and needle peening, in which first two are classified as the geometry improvement methods while

* Corresponding author.
E-mail address: halid.yildirim@cae.au.dk (H.C. Yıldırım).

https://doi.org/10.1016/j.ijfatigue.2023.107996
Received 29 August 2023; Received in revised form 18 September 2023; Accepted 8 October 2023
Available online 12 October 2023

Nomenclature

a	reference dimension for selecting the maximal FE size d for PSM application
d	average FE size of adopted mesh pattern
f_y	Yield strength
$f_{y,o}$	Reference yield strength
f_u	Tensile strength
E	Young's modulus of material
$c_{wi,i=1,2,3}$	coefficient depended on the stress ratio
FAT	The IIW fatigue class, i.e. the nominal or effective notch stress range in mega pascals corresponding to 95% survival probability at 2×10^6 cycles to failure (a discrete variable with 10–15% increase in stress between steps)
K_s	Stress concentration factor
FE	Finite element
m_1	Slope of the S-N line for stress cycles above the knee point
m_2	Slope of the S-N line for stress cycles below the knee point
$K_{i,i=1,2,3}$	Notch Stress Intensity Factors (NSIFs) for Mode I, II and III
K^j_{FE}	Calibration constants related to Mode I,II and III, j =*, **, ***
R	Nominal stress ratio ($\sigma_{min}/\sigma_{max}$)
R_0	size of structural volume in which the SED is averaged
r_0	distance between the point where the principal stress is maximum along the notch edge and the centre of the structural volume for averaged SED evaluation
k_σ	the calibration function to account for minimising the scatter
λ_i	Williams' eigenvalues
N_f	Cycles to failure
ΔS	Nominal stress range
t	Plate thickness of the specimen
ρ	Radius
2α	the notch opening angle
σ	Nominal stress (linear-elastic)
σ_N	Standard deviation in Log(N_f)
ν	Poisson's ratio
$\sigma_{\theta\theta,\theta=0}\tau_{r\theta,\theta=0}, \tau_{\theta z,\theta=0}$	The peak nodal stresses detected at the V-notch profile
Φ	the inclination angle
$SENE$	The strain energy value
$W_{FEM,i}$	strain energy calculated for the i-th finite element belonging to the control volume, V
W_{FEM}	averaged SED calculated by the 'direct approach'
$\bar{W}$	averaged SED

Subscripts

k	Characteristic value corresponding to 95% survival probability at 2×10^6 cycles to failure (continuous variable)
f	Effective
m	Mean value corresponding to 50% survival probability at 2×10^6 cycles to failure
max	maximum value
n	Notch stress
w	The notch factor or limit of a weld defined as the ratio of the ENS to SHSS

others are classified as the residual stress modification techniques. In the latter ones, the aim is to eliminate the high tensile residual stress in the weld toe region and induce compressive residual stresses at the weld toe in addition to the modifying the weld geometry. These all methods result in a reduced stress concentration at the weld toe.

High-frequency mechanical impact (HFMI) has significantly developed as a reliable, effective, and user-friendly method for PWT technique for welded structures [7–9]. The technique is effective since it allows to use high strength steel grades while maintaining the fatigue properties at the weld, i.e., the degree of the fatigue strength improvement increases with increasing yield strength. An analytical expression taking into account the material yield strength was derived, and verified by the experimental data at first in [7] and followed by [10–13]. The observations were based on the laboratory scale testing for extensive CAL with some VAL conditions. While the new HFMI recommendations take into account the effects of applied stress ratio [14], no separate methods were proposed for the misalignment effects other than the already recommended ones by Hobbacher [15].

There is literature available on the effect of misalignments on the fatigue strength of as-welded joints, well presented by Andrews [16], which is also the basis of British Standard PD 6493:1991. It was suggested that misaligned cruciform welds should be assessed for fatigue failure from the weld toe using the same K_s as for a butt weld with the same misalignment. For failure through the throat, an alternative expression for the K_s was recommended. Iida and Iino [17] investigated butt welds regarding the angular distortion effect. They applied preloading prior to the fatigue testing and compared the results to those without preloading, where an increase fatigue strength was found in the high applied loads, but less improvement was observed in the lower loads. Nguyen and Wahab [18] showed that the misalignment effect can be beneficial for high-cycle fatigue of the order of greater than 2×10^5 cycles, especially when compressive residual stresses are present by inducing surface treatment (i.e. HFMI). In this case, the improvement of fatigue strength of misaligned joints and undercut-free joints can be 50% more effective than that of aligned undercut joints. Xing and Dong [19] presented an analytical method for K_s calculation in a fillet-weld joint configuration containing either axial or angular misalignment between two intercostal members through an application of Castigliano's second theorem. A more recent work by Ahola et al. [20] investigated the effect of symmetry and loading type for non-load carrying joints with experimental fatigue tests and FE. The fatigue strength of asymmetric T-joints was higher than the ones for symmetric X-joints under axial loading. The symmetry of the joint increased the notch effect at weld toe which resulted in lower fatigue resistance. An improvement of fatigue strength was proven in bending loaded asymmetric T-joints and symmetric X-joints. The first comparison for of as-welded and HFMI-treated welds were conducted by Ottersbö ck [21] in which a complex interaction between the applied axial load, initial specimen distortion and the local stress field was found. Estimating the local stresses featured by an acting local stress range and the stress ratio. The use of distortion factor enabled a uniform SN-curve with a reduced scatter band. But the work was only limited to the constant amplitude fatigue loading as similar to the earlier studies in the field.

To perform an accurate fatigue life estimation, it is necessary to couple the misalignment effects with the real life load scenarios in the assessment. To our best knowledge, this has not been investigated for HFMI welds yet. Therefore, in this study, we present an empirical

solution to quantify the factors that affect the weld fatigue due to the misalignment. We organise the paper as follows. Firstly, a brief methodology is presented for the used local approaches. Second, the experimental results are presented for the load carrying cruciform joints that are improved by HFMI method. Then, several hypotheses are presented to quantify the misalignment effect by using the local assessment methods based on the real weld geometry. Extensive FE analyses results are presented for models with and without any misalignment effects. Finally, factors to determine the misalignment effects are presented with the proposed empirical relations.

2. Approaches to assess the weld fatigue

2.1. Structural hot spot stress (SHSS) approach

The structural stress σ_{hs} at the hot spot considers stress raising effects of structural detail without including the non-linear peak stress due to the local notch, i.e. the weld toe rounding is excluded from the structural stress. The SHSS value depends on the global dimension of the joint and on the loading parameters in near the welded joint. This value is defined on the surface at the hot spot of the weld. The SHSS approach is suitable for the structures that are characterised by structural discontinuities and geometric complexity when it is difficult to define the nominal stress acting the area of interest.

The SHSS approach is evaluated on the exterior surface, where the non-linear peak is dismissed by extrapolation of the stresses taken from selected reference points or a value obtained through the plate's thickness. For SHSS, the different nominal FAT classes are proposed in two FAT classes, FAT 90 and FAT 100, for load and non load carrying welded joints. These curves are referred to as-welded condition unless stated otherwise. They include only small effects of misalignment. In the presence of a consistent misalignment, a stress magnification factor K_m, defined by IIW guideline [15], must be included. The design value of the SHSS range $\Delta\sigma_{hs}$ must be minor to $2 \cdot f_y$ to avoid plastic yielding. Detail calculation steps are provided in IIW recommendations [15] but it is necessary to provide recent suggestions published in the literature by [22]. The extrapolation of the hot spot stress value can be executed with the using of both fine and coarse meshes. It is possible to detect the first principal stress in the reference points and the stress along x-axis. For 2D models, the *mapped-mesh* algorithm can be used to create the mesh with four-node linear plane elements (PLANE 182 in ANSYS®). For 3D models, eight-node or twenty-node linear hexahedral elements are adopted for the mesh generation (SOLID185 and SOLID 186 in ANSYS®). For the eight-node, several elements are used thru the main plate thickness. For the twenty-node, only one element is used to avoid any singularity.

2.2. Effective notch stress (ENS) approach

Effective notch stress is the total stress at the root of a notch and in this method the maximum principal stress or von Mises stress at the notch, e.g. weld toe or root, can be idealised by considering a linear-elastic material behaviour through the finite element analysis.To consider the non-linear material behaviour at the notch root and also to include shape effects of the weld, the weld profile at weld toe or root is replaced by a fictitious notch radius. This method is applicable for plates that are characterised by a thickness $t \geq 5$ and for these welds, it is suggested that:

$$\rho_f = \rho + 1 \text{ mm} \tag{1}$$

where ρ is the actual radius of the weld toe, ρ_f is the effective radius which is implemented to the finite element model. For the worst case scenario, the actual radius ρ is assumed equal to zero. Thus, the equation is reduced to $\rho_f = 1$ mm at weld toe or root. This value may be smaller for the thinner welded joints [23]. The ENS approach is suitable to investigate welded joints at the weld toe or weld root. This is the biggest advantage of ENS and can be assessed with the related fatigue class. The effective notch stresses can be obtained by finite element model. In this case the IIW recommends global element size and mesh pattern which are detailed in [3]. Only one fatigue class is given as FAT 225 for the assessment of as-welded joints.

2.3. Notch stress intensity factors (NSIFs) approach

The linear elastic fracture mechanics (LEFM) theory was extended to study the weld fatigue. The theory of NSIFs, elaborated by Gross and Mendelson (1972) [24], where the weld toe profile was considered as a sharp V-notch with a tip radius equal to zero ($\rho = 0$) and the weld root was considered like a pre-crack in the weld. The V-notch is usually in three different modes: Mode I: tensile opening; Mode II: in-plane shear; Mode III: out-of-plane shear. For instance, a V-notch is subjected to Mode I and II in plane problems, from which the intensities can be evaluated associated to the each Mode.

The work of Lazzarin and Tovo in 1998 [4] let the use of NSIFs approach with one FAT value. The NSIFs approach proposes a fatigue design curve $K_1 - N_f$ for different joint's geometries because the shape and size effects are already accounted by the stress intensity K_1.

On the other hand, the NSIFs approach have some disadvantages [25]. Intensive refine meshes are required to calculate the NSIFs and thus the computational time increases. Stress distributions are required to calculate K_i and so the post-process operation can be complex and time consuming. The unit of measurement of $K_{i,i=1,2,3}$ are expressed in [MPa] $\text{m}^{1-\lambda_{i,i=1,2,3}}$, so it changes with the singularity of the stress distribution that depends on the opening angle 2α. Due to this, the comparison of stress field between V-notch with different opening angle is not possible.

2.4. Strain energy density (SED) approach

Lazzarin and Zambarndi [5] proposed a strain energy criterion to overcome the limits of NSIFs approach. SED is based on the structural volume according to Neuber's theory. Indeed materials are sensitive to the average stress state in a structural volume that can be characterised as the material's property. That is, SED uses as critical parameter defined for a circular sector of R_0 as a material property to evaluate the structural resistance. The typical values of R_0 are *0.28mm* for steel structures and *0.12mm* for aluminium alloys. Initially, the method was calibrated only for Mode I loading [5], but subsequently it was extended also for Mode II and III. Under plane strain hypothesis, the averaged SED inside a structural volume of radius R_c is expressed as function of NSIFs for Mode I and II for a V-notch, characterised by a opening angle 2α in Eq. (2):

$$\bar{W} = \frac{1}{E} \cdot \left(c_{w1} \cdot e_1 \cdot \frac{K_1^2}{R_0^{1-\lambda_1}} + c_{w2} \cdot e_2 \cdot \frac{K_2^2}{R_0^{1-\lambda_2}} + c_{w3} \cdot e_3 \cdot \frac{K_3^2}{R_0^{1-\lambda_3}} \right) \tag{2}$$

where $K_{i,i=1,2,3}$ are the Notch Stress Intensity Factors (NSIFs) for Mode I, II and II, R_0 is the radius of structural volume, E is the Young modulus; $c_{wi,i=1,2,3}$ are the coefficient that they depend on the stress ratio $R = \frac{\sigma_{min}}{\sigma_{max}}$ and are provided in Ref. [26], $e_{i,i=1,2,3}$ are the parameters to consider the dependence on the opening angle 2α of V-notch and also on the Poisson's ratio ν. The value of $e_{i,i=1,2,3}$ are defined in [27,28] as function of the opening angle and for steel $\nu = 0.3$:

The averaged SED can be obtained by FE method; the energy of each element is summed and divided by the structural volume as given by Eq. (3).

$$\Delta\overline{W}_{FEM} = \frac{\sum_{V(R_0)} W_{FEM,i}}{V(R_0)} \tag{3}$$

This approach is called "direct approach" and the unit is $\left[\frac{\text{MJ}}{\text{m}^3}\right]$ or $\left[\frac{\text{J}}{\text{mm}^3}\right]$. The SED approach has several advantages. The comparison of stress field between V-notch with different opening angle is possible

because the fatigue resistance is expressed in terms of energy, so the unit of measure remain constant. Similar to the NSIFs approach, the design fatigue curve is unique and in terms of strain energy. Relativity coarse mesh can be employed in SED.

2.5. Peak stress method (PSM)

The PSM is an approach that allows to determine the value of NSIFs rapidly to assess the weld fatigue. The PSM is based on FE analysis with coarse mesh and it does not require a refined mesh in correspondence of the V-notch. Similarly in SED, PSM overcomes the limits of NSIFs' approach. The method is applicable to steel structures and aluminium alloys and provides correlations between the Mode I,II and III NSIFs and the corresponding peak stress components (see Eqs. (4)–(6)):

$$K_1 \cong K_{FE}^{*} \cdot \sigma_{\theta\theta,\theta=0,peak} \cdot d^{1-\lambda_1} \tag{4}$$

$$K_2 \cong K_{FE}^{**} \cdot \tau_{r\theta,\theta=0,peak} \cdot d^{1-\lambda_2} \tag{5}$$

$$K_3 \cong K_{FE}^{***} \cdot \tau_{\theta z,\theta=0,peak} \cdot d^{1-\lambda_3} \tag{6}$$

where $K_{FE}^{*}, K_{FE}^{**}, K_{FE}^{***}$ are the calibration constants related to Mode I,II and III and depend on the element type, the software type, the mesh conformation and the nodal stress evaluation method. $\sigma_{\theta\theta,\theta=0,peak}$ $\tau_{r\theta,\theta=0,peak}, \tau_{\theta z,\theta=0,peak}$ are the peak nodal stresses at the V-notch d is the global element size, $\lambda_1, \lambda_2, \lambda_3$ are the Williams' eigenvalues. In plane strain, the averaged SED calculated by Eqs. (2), can be rewritten as function of the peak stresses $\sigma_{\theta\theta,\theta=0,peak}, \tau_{r\theta,\theta=0,peak}, \tau_{\theta z,\theta=0,peak}$ by using Eqs. (4)–(6) and the imposing the following relation:

$$\bar{W} = (1-\nu^2) \cdot \frac{\sigma_{eq,peak}^2}{2E} \tag{7}$$

where the $\sigma_{eq,peak}$ is defined as a function of the peak stresses as follows:

$$\sigma_{eq,peak} = \sqrt{f_{w1}^2 \cdot \sigma_{\theta\theta,\theta=0,peak}^2 + f_{w2}^2 \cdot \tau_{r\theta,\theta=0,peak}^2 + f_{w3}^2 \cdot \tau_{z\theta,\theta=0,peak}^2} \tag{8}$$

where $f_{wi,i=1,2,3}$ are the peak stresses correction factors and are defined as follows:

$$f_{wi} = K_{FE}^{j} \cdot \sqrt{\frac{2e_i}{1-\nu^2}} \cdot \left(\frac{d}{R_0} \right)^{1-\lambda_i} \Bigg|_{\substack{i=1,2,3 \\ j=*,**,***}} \tag{9}$$

PSM has some advantages. The comparison of stress field between V-notch with different opening angle is possible because the fatigue resistance is expressed in terms of equivalent peak stress, so the unit of measure remain constant. As in the NSIFs and SED, the design fatigue curve is unique. The post-process analysis require only one nodal peak stress instead of a large number of stress distance values. FE analysis require a coarser mesh than that of NSIFs and SED approaches. The global element size d can be higher than the control radius R_0, unlike the "direct approach" to calculate the SED where $d < R_0$. The modelling of the control volume to calculate the averaged SED is not necessary. Besides these advantages, there are some precautions that must be taken. The PSM calibration constants are not calibrated for V-notch opening angle higher than 135°, but recently for ten-node tetra elements the PSM constants has been calibrated up to 180°. When the PSM estimates a crack initiation in a singularity region that is different from the experimental one, the $\Delta\sigma_{eq,peak}$ related to effective area must be calculated. Last but not least, special attention shall be taken for the weld toe radius ρ [29,30];

- $\rho < 1.5$–1.8 mm, the weld toe radius can be considered equal to 0 mm, so to have the worst possible case: V-notch;
- $1.8 < \rho < 4$ mm, this is the case of blunt notch, so the PSM is applied in combination with SED approach;
- $\rho > 4$ mm, the classical mechanical point criterion is used for fatigue assessment

3. Misalignment investigations

3.1. Definitions

The weld fatigue can be significantly influenced by joint misalignments which introduce a secondary bending at the presence of axial tension. There are two different types of misalignment defined: the axial misalignment e, and the angular misalignment α, as shown in Fig. 1, [19]. In Section 3, α was used whereas in Section 4, e was used dominantly (see Fig. 2, [31]).

3.2. Experimental procedure to determine the misalignment effect

The mechanical properties and the chemical composition of the steel grade AH36 with 6 mm thickness are given in Tables 1 and 2. Load-carrying cruciform joints were produced from the welded steel plates, Fig. 3. High Frequency Mechanical Impact (HFMI) treatment was applied at the welds before producing the specimens.

Geometry measurements were carried out by using an ATOS Scan-box from GmbH with an optical measuring accuracy of 0.02 mm. Thirteen points clouds were obtained from the measurements, that is one set for each specimen. Each welded joint was then modelled by extracting the geometrical dimensions from the points cloud. To dimension the geometry, the points coordinates are read into MatLab. The obtained data was very large for each test sample. Thus, a *sampling parameter* was introduced to reduce and simplify the data while keeping its reliability by conducting sensitivity analyses. The number of the data points were reduced by setting the sampling parameter to ten. That is, every tenth point was taken and used to build the FE models. The sampling parameter was acceptable based on the sensitivity analysis. If the parameter changed, the maximum principal stress at the weld toe would be stable, as presented in Fig. A.17. The obtained point cloud helped define the specimens' dimensions. To visualise better, the geometrical parameters were defined as shown in Fig. A.18. The specimen dimensions are reported in Table A.18. Following the geometrical dimension, the angular misalignment, α was calculated by $\alpha = \tan^{-1} m$ where m is the angular coefficient of the largest distance away from the attachment centreline. The results of the angular misalignment are reported in Appendix Table A.18.

Specimens were fatigue tested under Variable Amplitude Loading (VAL) at a stress ratio of R = −0.43. The applied stress history was the same as reported in the works of [13] and [32]. The loading history included 250,000 cycles distributed between fourteen different amplitudes. The cycle amplitude distribution was approximately linear on a semi-log plot. The amplitude of the smallest applied load cycle was 16% of the maximum load cycle. The order of the individual cycles within the 250,000 spectrum was randomly chosen and each cycle had a stress ratio of $R = -0.43$. Here, the aim was to perform fatigue testing at a stress ratio that would provide considerable amount of residual stresses relaxation and would avoid buckling of specimens under overloads close to the yield strength of material. Depending on the load range, fatigue tests were performed at an average cyclic frequency of around 4–10 Hz. During the testing, the applied load history was continuously monitored to ensure that the desired history matched the true applied history. The results are provided in Table 3.

3.3. Finite element analysis to calculate $\Delta\sigma_{11,max,weldtoe}$

The obtained points cloud were imported to Ansys® APDL to model 2D specimen geometries and to perform FE analyses. Full specimen geometries were used without any symmetry condition due to the misalignments. The same boundary conditions were used as given by the Ref. [33]. The specimen was allowed to move in the applied load direction only and fixed at the one end to prevent the rigid body motion. The models were meshed with a global element size equal to

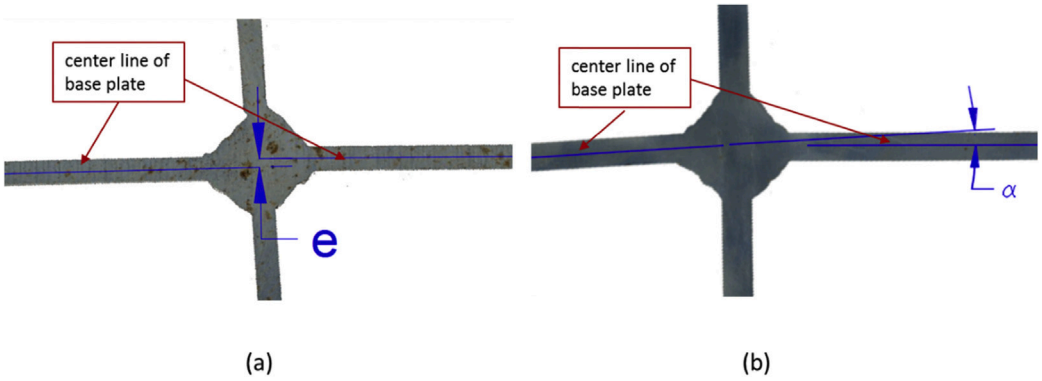

Fig. 1. Definition of two types of joint misalignment in fillet welded connection: (a) axial misalignment; (b) angular misalignment [19].

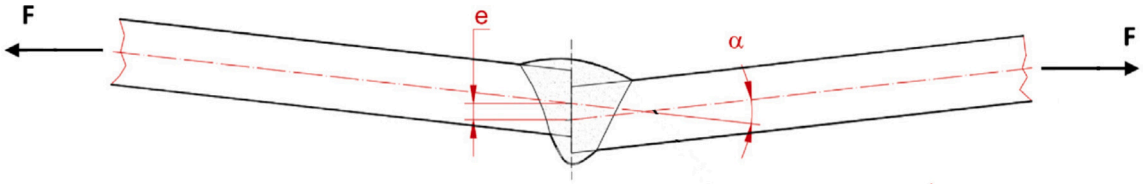

Fig. 2. Definition of two types of joint misalignment in butt welded connection [31].

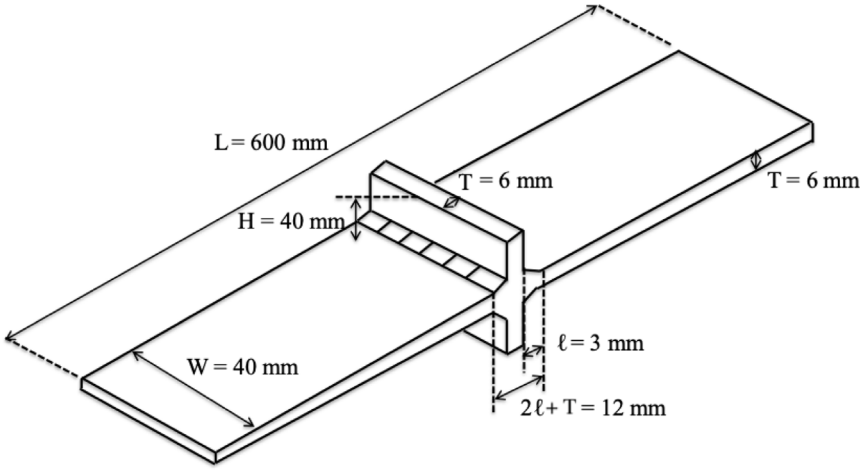

Fig. 3. Schematic view of the specimen tested under variable amplitude loading.

Table 1
Mechanical properties of the tested steel AH36.

Material	Yield strength f_y [MPa]	Ultimate strength f_u [MPa]	Elongation [%]	Young modulus [MPa]	Poisson's ratio ν
AH36	423	546	0	206000	0.3

Table 2
Chemical composition of the tested steel AH36.

Material	C	Si	Mn	P	S	Al	Nb	V	Ti	Cu	Cr	Ni	Mo	Ca
AH36	0.14	0.39	1.43	0.008	0.007	0.034	0.013	0.008	0.04	0.021	0.08	0.06	0.007	0.0

0.5 mm. The specimens were subjected to a tensile stress of σ_{nom} = 1 MPa at the end, see Fig. 4.

A typical boundary and loading condition of the model is given in Fig. 4, while the first principal stress can be observed in Fig. 5 for the applied tensile stress of 1 MPa. The results of FE analysis for each specimen are tabulated in Table 3.

3.4. Reference models and local approaches

Two reference models were created for both as-welded and HFMI treated conditions. The models were built without any misalignment and with a sharp V-notch at the weld toe, where the HFMI groove geometry was profiled for the treated case. As there is no misalignment assumed for the reference model, a double symmetry is utilised; i.e., only 1/4 of the joint is created. Effective Notch Stress (ENS) approach and Structural Hot-Spot Stress (SHSS) approach, and the PSM approach were performed, where the latter one was combined with the SED for the HFMI case.

In what follows is the brief descriptions of used local methods. For each local assessment approach, example evaluations are given however due to the large number of evaluations all the results are detailed in A.19–A.22.

Table 3
Results of fatigue testing and finite element analyses of the specimens with angular misalignment.

Specimen	σ_{max} [MPa]	σ_{min} [MPa]	$\Delta\sigma$ [MPa]	N_f [cycles]	$\Delta\sigma_{11,max,weldtoe}$ [MPa]	Right misalignment α_R [°]	Left misalignment α_L [°]	Failure
355-WH-2	258.33	−116.67	375.00	2 799 750	5.7937	1.16	1.48	Gusset
355-WH-3	258.33	−116.67	375.00	3 387 000	5.7993	1.03	1.42	Gusset
355-WH-5	233.33	−100.00	333.33	3 410 280	5.8974	0.91	1.32	Gusset
355-WH-8	200.00	−83.33	283.33	8 750 324	4.5343	0.87	1.27	Gusset
355-WH-14	175.00	−75.00	250.00	6 673 500	4.92	0.64	1.25	Gusset
355-WH-16	175.00	−75.00	250.00	7 085 250	5.4915	0.78	1.29	Gusset
355-WH-17	200.00	−83.33	283.33	4 420 500	5.0055	0.80	1.23	Gusset
355-WH-18	233.33	−100.00	333.33	3 607 500	5.0221	0.86	1.24	Gusset
355-WH-20	233.33	−100.00	333.33	3 261 000	4.6786	0.86	1.07	Gusset
355-WH-21	200.00	−83.33	283.33	4 446 750	4.5449	0.96	1.01	Gusset
355-WH-22	258.33	−116.67	375.00	2 341 500	4.4553	1.01	0.94	Gusset

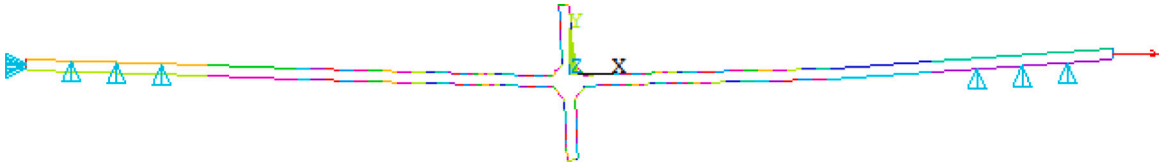

Fig. 4. A typical boundary and load condition of the model. The red arrow represents the applied stress.

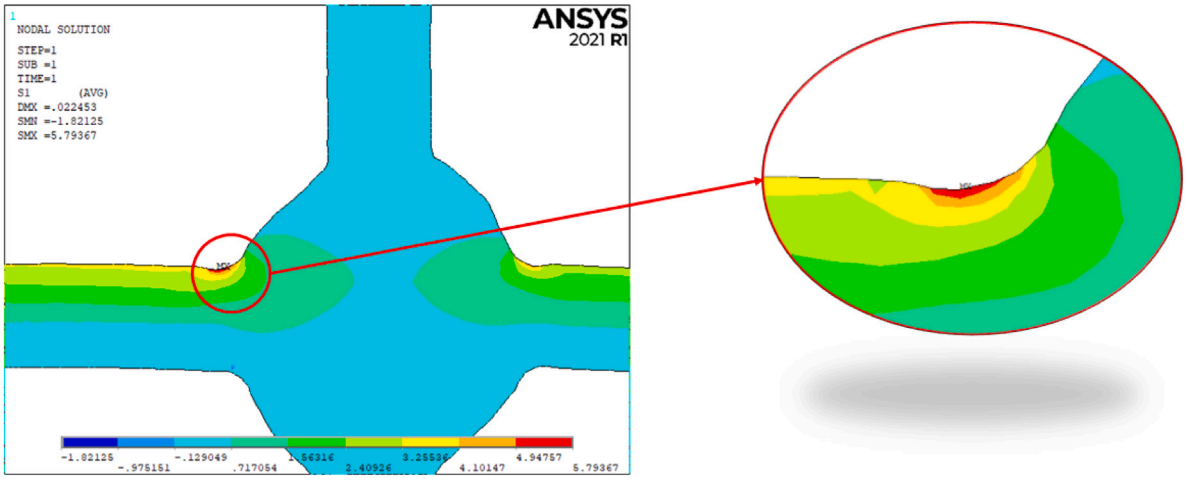

Fig. 5. Contour plots of the first principal stress following $\sigma_{nom} = 1$ MPa for an HFMI-treated weld.

3.4.1. SHSS

The hot-spot stress was extrapolated at two reference points placed at 0.4t and 1.0t distance from the weld toe tip, thus at 2.4 mm and 6 mm. These reference points were used for the hot-spot type a. For type b, the structural hot-spot stress was extrapolated at three reference points located at 4 mm, 8 mm and 12 mm distance from the weld toe. The four-node linear element PLANE 182 is chosen in Ansys®APDL with plane strain.

3.4.2. ENS

To apply ENS approach, the IIW recommendations for the global element size and mesh pattern were followed [3]. The weld toe radius of $\rho_f = 1$ mm was used as the actual radius ρ was assumed zero for the worst case. The weld roots for non-penetrating fillet welds were modelled with U shaped notch as recommended by [34]. Two different analysis were done:

1. The first one was characterised by the using of 4-node linear element PLANE 182 with *Simple Enhanced Strain* as Key Option 1 and *Plane Strain* as Key Option 3;
2. The second one was characterised by the using of 8-node quadratic element PLANE 183 with *Quadrilateral* as Key Option 1, *Plane Strain* as Key Option 2 and *Pure Displacement* as Key Option 6.

3.4.3. PSM

The PSM was used in two different ways to assess the as-welded and treated states. The modelling procedures for the PSM methods were the same as the ones presented by [35].

PSM for reference model with sharp V-notch. The model was 2D structure with the adoption of four-node linear elements. The element PLANE 182 was chosen from the Ansys®APDL library with *Simple Enhanced Strain* as Key Option 1 and *Plane Strain* as Key Option 3. The root was characterised by an initial opening length equal to 0.1 mm. The weld toe was subjected to pure Mode I as it was modelled by a V-notch opening angle 2α equal to 135°. The root was a V-notch opening angle equal to 0°, thus it was subjected to Mode II in addition to Mode II. For Mode I and Mode II, the PSM requirements are defined in Table 4. The PSM calibration constants were equal to $K^*_{FE} = 1.38 \pm 3\%$, $K^{**}_{FE} = 3.38 \pm 3\%$ for Mode I and II, respectively. The element size was obtained as 0.2 mm by the following. The ratio $(a/d)_{min}$ was determined for Mode I and Mode II, from the literature and the higher was chosen. The value of a was the reference dimension to determine the maximal FE sizes d and was defined as $0.5t$. The minimum element size was calculated by $d_{min} = a/14 = 6/14 = 0.214$ mm.

The λ_1, e_1, λ_2 and e_2 values are depended on the V-notch opening angle 2α, that is 135° for the weld toe and 0° for the root, see Table 5:

Table 4
Requirements for PSM.

Element type	Mesh algorithm	*Mode I*			
		$(a/d)_{min}$	2α	Mesh Pattern $2\alpha < 90°$	Mesh Pattern $2\alpha > 90°$
Plane 182 KeyOpt:*Simple Enhanced Strain + Plane Strain*	Free	3	$0° < 2\alpha < 135°$	Four adjacent elements share the same node	Two adjacent elements share the same node
		Mode II			
Plane 182 KeyOpt:*Simple Enhanced Strain + Plane Strain*	Free	14	$0° < 2\alpha < 135°$	Four adjacent elements share the same node	Four adjacent elements share the same node up to $2\alpha = 102.5°$

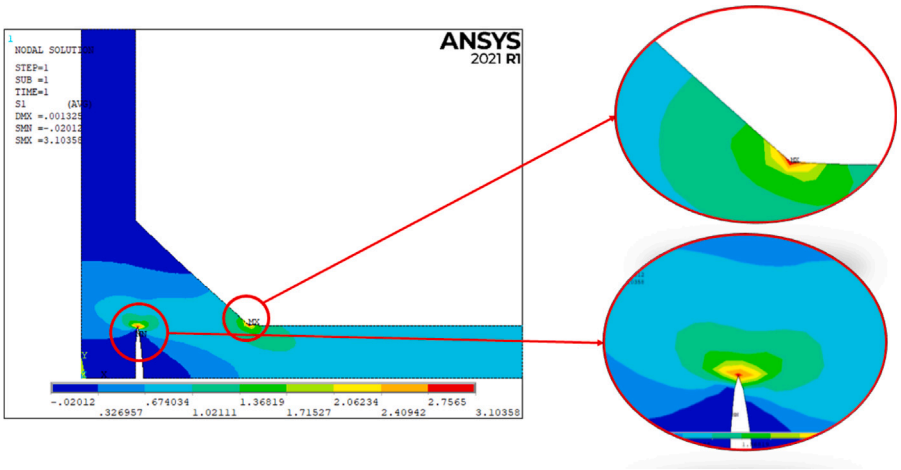

Fig. 6. Plot of 1st principal stress for an external applied nominal stress range of 1 MPa for PSM.

Table 5
Value of λ_1, e_1, λ_2 and e_2 as a function of the opening angle 2α.

2α [°]	λ_1 (Mode I)	e_1 (Mode I)	λ_2 (Mode II)	e_2 (Mode II)
135°	0.674	0.117	/	/
0°	0.5	0.133	0.5	0.341

Table 6
Values of the corrective stress factors f_{w1} and f_{w2} as a function of the opening angle 2α.

2α [°]	f_{w1}	f_{w2}
135°	0627	/
0°	0.633	2.473

Table 7
Dimensions of the HFMI groove.

Depth [mm]	ρ_{HFMI} [mm]	Width [mm]	2α[°]
0.3	3.31	4.48	135

The corrective stress factors for Mode I and II were calculated with Eq. (9) for the weld toe and root, Table 6. The first principal stress is shown in Fig. 6:

Two local reference systems were created to represent the weld toe and the root apex. The work plane was rotated 112.5° for the toe and 90° for the root. By using the local reference system, the stress component $\Delta\sigma_{yy}$ was obtained. Then the equivalent peak stresses were calculated by Eq. (8).

$$\Delta\sigma_{eq,peak,toe} = f_{w1} \cdot \sigma_{\theta\theta,\theta=0,peak} = 1.946 \text{ MPa} \tag{10}$$

The results are reported in the Appendix A.21.

PSM for reference model with the HFMI groove. PSM was used in combination with the SED approach with the adoption of four-node linear elements, considering only the weld toe. Table 7 provides the HFMI groove dimensions based on the literature [12].

The element PLANE 182 is chosen from the Ansys®APDL library with *Simple Enhanced Strain* as Key Option 1 and *Plane Strain* as Key Option 3. The SED approach for blunt notches is based on the creation of a structural volume at the weld toe, that can be rigidly rotated to included the whole maximum principal stress, which is related to the highest strain energy density. Therefore, the inclination angle Φ was determined with respect to the blunt notch bisector of the most stressed area. To find the inclination angle, the model was meshed with a global element size. The model was subjected to an external nominal stress $\Delta\sigma_{nom} = 1$ MPa applied on the main plate. One aspect was that the highest stress was not at the blunt notch bisector, so it was matter of quantifying the grades of rotation. Clockwise rotation about the global z-axis was done by $\Phi = 2.411°$.

The circular sector was created according to Neuber's parameters, in which 2α is the notch opening angle, ρ is the notch radius, r_0 is the distance between the origin of the analytical frame and the notch tip.

$$q = \frac{2\pi - 2\alpha}{\pi} = 2 - \frac{135}{180} = 1.25 \tag{11}$$

$$r_0 = \frac{q-1}{q} \cdot \rho_{HFMI} = \frac{1.25-1}{1.25} \cdot 3.31 = 0.662 \text{ mm} \tag{12}$$

$$R_0 + r_0 = 0.28 + 0.662 = 0.942 \text{ mm} \tag{13}$$

The control volume to calculate the averaged SED was created. To generate the mesh, elements inside the structural volume were characterised by global element size of 0.01 mm with free-mesh algorithm.

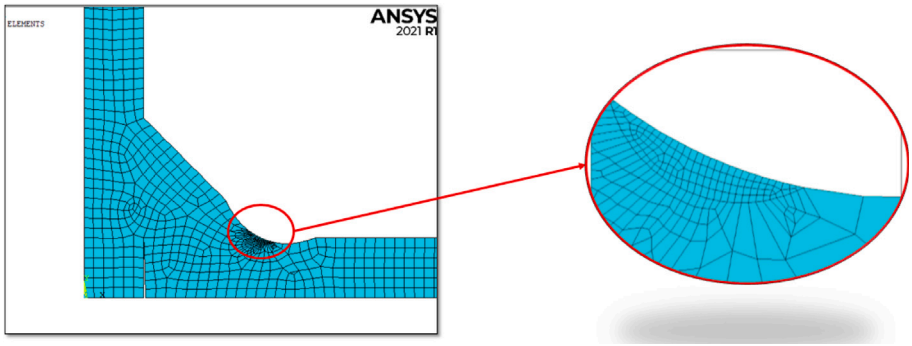

Fig. 7. Mesh of the weld profile and the structural volume.

The other areas were meshed by global element size of 0.1 mm, see Fig. 7. In both cases, free mesh was chosen.

The averaged SED is defined as the energy inside the structural volume. The model was subjected to a nominal stress of 1 MPa. Eq. (2) was applied to calculate the SED value. That is, $SED = \frac{SENE}{VOLU} = \frac{1.84529 \cdot 10^{-6}}{0.294241} = 6.2713 \cdot 10^{-6} \frac{\text{MJ}}{\text{m}^3}$, then the equivalent peak stress was obtained by Eq. (14).

$$\Delta\sigma_{eq,peak} = \sqrt{\frac{2 \cdot E \cdot SED}{1-\nu^2}} = \sqrt{\frac{2 \cdot 206000 \cdot 6.2713 \cdot 10^{-6}}{1-0.3^2}} = 1.685 \text{ MPa} \tag{14}$$

Subsequently, the equivalent peak stress at the weld root is calculated by the same procedure used for the reference model for the sharp V-notch. Thus, the results are $\Delta\sigma_{yy,root} = 2.93004$ MPa and $\Delta\tau_{xy,root} = 0.331525$ MPa.

The equivalent peak stresses were calculated by Eq. (8).

$$\Delta\sigma_{eq,peak,root} = \sqrt{f_{w1}^2 \cdot \sigma_{\theta\theta,\theta=0,peak}^2 + f_{w2}^2 \cdot \tau_{r\theta,\theta=0,peak}^2} = 2.028 \text{ MPa} \tag{15}$$

All the results are reported in the Appendix A.22.

3.5. The models with misalignment

To determine the misalignment effect, models with angular misalignment were created by using the real geometries obtained from point cloud per specimen. The application of the local approaches were the same as described in the previous Section 3.4. All the analyses results are provided in A.23–A.26.

But for the sake of guidance, examples with the misalignment for the ENS and SHSS approach are provided below.

3.5.1. ENS approach

The worst case scenario was applied, i.e., $\rho_f = 1$ mm. The weld roots for non-penetrating fillet welds were modelled with U shaped notch [34]. The model mesh included global element size 0.1 mm with PLANE 182. The results of the first principal stress are shown in the Fig. 8, for an external applied pressure equal to 1 MPa:

The maximum first principal stress at the weld toe and root were $\Delta\sigma_{11,Toe,max} = 6.4756$ MPa and $\Delta\sigma_{11,Root,max} = 3.9549$ MPa.

3.5.2. SHSS approach

For type *a*, the hot-spot stress was extrapolated at two reference points $0.4t$ and $1.0t$ away from the weld toe tip. For type *b*, the structural hot-spot stress was extrapolated at three reference points located at 4 mm, 8 mm and 12 mm away from the weld toe. The used element size was 0.4 mm. A typical mesh and extrapolation points are shown 9.

For an external applied pressure $\Delta\sigma_{nom} = 1$ MPa, the results of the tension at the reference points for hot spot type *a* are calculated and resultant SHSS are provided in Table A.23.

4. Factors to determine the misalignment effect

4.1. Definitions

Following the FE analysis of the models with and without angular misalignment, six-factors were evaluated to determine the misalignment effect and to understand the advantages of HFMI treatment for experimental data obtained at VAL. These factors are obtained from the evaluations based on the equivalent peak stress, the hot-spot stress and the effective notch stress. The factors are summarised below but the detailed values are provided in Tables B.27–B.32. The factors tell us only the comparison in between the used stress analyses based on the real geometry and the corresponding reference joint geometry.

1. The first factor is the ratio between the maximum equivalent peak stress between the root and the weld toe in the reference model with angular misalignment and the maximum equivalent peak stress between the root and the weld toe in the reference model without angular misalignment:

$$Factor_1 = \frac{\Delta\sigma_{max,eq,peak,between-root-and-toe-with-Misalignment}}{\Delta\sigma_{max,eq,peak,between-root-and-toe-without-Misalignment}} \tag{16}$$

2. The second factor is the ratio between the effective notch stress, calculated with the elements PLANE 182, at the weld toe in the reference model with angular misalignment and the effective notch stress, calculated with the elements PLANE 182, at the weld toe in the reference model without angular misalignment:

$$Factor_2 = \frac{\Delta\sigma_{11,max,toe-with-Misalignment,PLANE182}}{\Delta\sigma_{11,max,toe-without-Misalignment,PLANE182}} \tag{17}$$

3. The third factor is the ratio between the effective notch stress, calculated with the elements PLANE 183, at the weld toe in the reference model with angular misalignment and the effective notch stress, calculated with the elements PLANE 183, at the weld toe in the reference model without angular misalignment:

$$Factor_3 = \frac{\Delta\sigma_{11,max,toe-with-Misalignment,PLANE183}}{\Delta\sigma_{11,max,toe-without-Misalignment,PLANE183}} \tag{18}$$

4. The fourth factor is the ratio between the hot-spot stress type *a* of the reference model with angular misalignment and the hot-spot stress type *a* of the reference model without angular misalignment:

$$Factor_4 = \frac{SHSS_{LSE,with-Misalignment,type-a}}{SHSS_{LSE,without-Misalignment,type-a}} \tag{19}$$

5. The fifth factor is the ratio between the maximum first principal stress at the weld toe of the model obtained from the point cloud and the effective notch stress calculated with the elements PLANE 182, at the weld toe in the reference model without angular misalignment:

$$Factor_5 = \frac{\Delta\sigma_{11,max,toe,from-point-cloud-with-Misalignment}}{\Delta\sigma_{11,max,toe-without-Misalignment,PLANE182}} \tag{20}$$

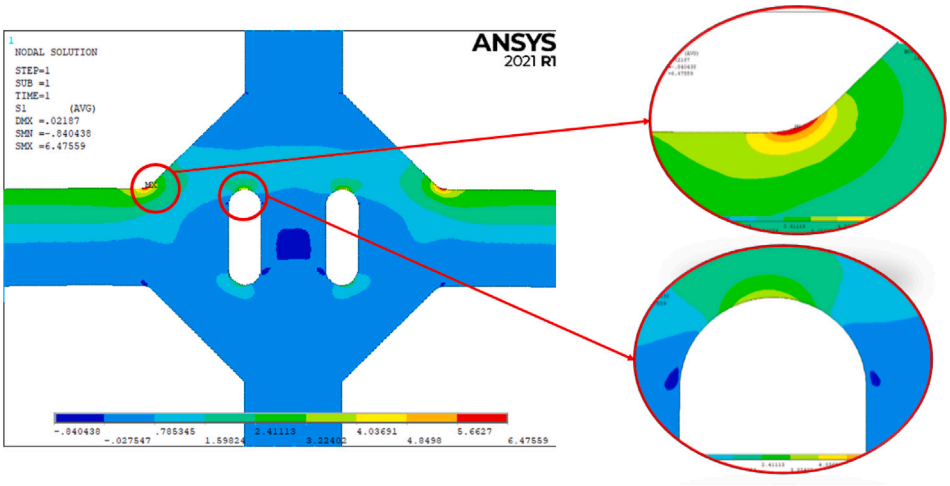

Fig. 8. Plot of the first principal stress of ideal model with angular misalignment with element PLANE 182.

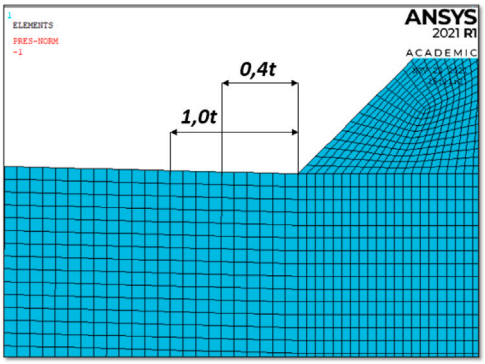

Fig. 9. Mapped mesh for SHSS approach and reference points.

6. The sixth factor is the ratio between the equivalent peak stress at the weld toe in the reference model with angular misalignment and with sharp V-notch, and the equivalent peak stress at the weld toe in the reference model with angular misalignment and with the HFMI groove:

$$Factor_6 = \frac{\Delta\sigma_{eq,peak,toe-with-Misalignment-sharp-V-notch}}{\Delta\sigma_{eq,peak,toe-with-Misalignment-HFMI-groove}} \tag{21}$$

4.2. Hypotheses to determine k_σ function

Following the definition of the different ratios, the aim was to obtain a k_σ function to detect the effect of the axial e and angular misalignment α. The procedure to define the expression of the k_σ function includes several hypotheses that considers the misalignment effect. These expressions are functions of the axial and angular misalignment and the thickness t. That is,

$$k_\sigma = f(e,t) \tag{22}$$

Additional calibration parameters, β and γ, are proposed to evaluate k_σ empirically by minimising the standard deviation σ_y of the experimental data. Similar approaches have been successfully performed in [7], [36] and [37] to account for several welding process parameters, e.g., the treatment, variations of the experimental test setup in different labs or weld quality.

The hypotheses to obtain the k_σ function is detailed as below steps:

1. The experimental data used for the evaluation of k_σ function were multiplied for the stress concentration factors calculated by FE methods for each specimen. The factors were obtained from the FE analysis, i.e., for actual geometry in Table 3 for the Effective Notch Stress method and for the PSM approach on the reference model with angular misalignment. Subsequently, these values were multiplied with the k_σ to obtain the resultant stress value σ_{max,k_σ}:

$$\sigma_{max,k_\sigma} = \sigma_{max} \cdot K_{s,actual/ENS/PSM} \cdot k_\sigma \tag{23}$$

2. The angular misalignment is converted to axial misalignment, i.e.,

$$e_{new} = \frac{l}{2} \cdot \tan(\alpha_{tot}) \tag{24}$$

where l is the total length of the sample and α_{tot} is the sum of the right and left angular misalignment. The results are reported in Table 8.

3. The hypotheses to estimate the k_σ functions are the following Eqs. (25)–(32):

$$k_\sigma = \gamma \cdot \left(1 + \beta \cdot \frac{e_{new}}{t}\right) \tag{25}$$

$$k_\sigma = \gamma \cdot \left(1 - \beta \cdot \frac{e_{new}}{t}\right) \tag{26}$$

$$k_\sigma = \frac{\gamma}{1 + \beta \cdot \frac{e_{new}}{t}} \tag{27}$$

$$k_\sigma = \gamma^{1-\beta \cdot \frac{e_{new}}{t}} \tag{28}$$

$$k_\sigma = \gamma^{1+\beta \cdot \frac{e_{new}}{t}} \tag{29}$$

$$k_\sigma = \gamma^{\frac{1}{1-\beta \cdot \frac{e_{new}}{t}}} \tag{30}$$

$$k_\sigma = \gamma^{\frac{1}{1+\beta \cdot \frac{e_{new}}{t}}} \tag{31}$$

$$k_\sigma = \gamma^{\beta \cdot \frac{e_{new}}{t}} \tag{32}$$

4. The two constants β and γ were systematically changed to determine which values would result in the minimum standard deviation σ_y for the experimental data. The range of variation for both vale was proposed as between 0.1 and 10 with a step-size of 0.05;
5. For each expression of the k_σ function, the minimum standard deviation σ_y, the corresponding T_σ and slope B were determined. The results are reported in the following section with the two statistical analysis conducted. The first one is with the free slope and the second one is with the fixed slope 5, that is the typical value of the design curve for HFMI treated welds.

Table 8
Axial misalignment values evaluated by Eq. (24).

Specimen	σ_{max} [MPa]	σ_{min} [MPa]	$\Delta\sigma$ [MPa]	N_f [cycles]	t [mm]	α_{tot} [°]	e [mm]
355-WH-2	258.33	−116.67	375.00	2 799 750	6	2.641	13.837
355-WH-3	258.33	−116.67	375.00	3 387 000	6	2.452	12.846
355-WH-5	233.33	−100.00	333.33	3 410 280	6	2.137	11.194
355-WH-8	200.00	−83.33	283.33	8 750 324	6	1.896	9.932
355-WH-14	175.00	−75.00	250.00	6 673 500	6	2.538	13.296
355-WH-16	175.00	−75.00	250.00	7 085 250	6	2.068	10.833
355-WH-17	200.00	−83.33	283.33	4 420 500	6	2.034	10.653
355-WH-18	233.33	−100.00	333.33	3 607 500	6	2.102	11.014
355-WH-20	233.33	−100.00	333.33	3 261 000	6	1.931	10.113
355-WH-21	200.00	−83.33	283.33	4 446 750	6	1.965	10.293
355-WH-22	258.33	−116.67	375.00	2 341 500	6	1.948	10.203

Table 9
Statistical analysis results for the actual model.

Equation for k_σ	*Free slope*					*Fixed slope*				
	σ_y	β	γ	T_σ	B (slope)	σ_y	β	γ	T_σ	B (slope)
(25)	0.1666	0.1	0.7	7.7736	1.0892	0.36503	0.1	5.35	2.661	5
(26)	0.1583	0.2	1.05	3.4863	1.6997	0.25609	0.25	2.15	1.987	5
(27)	0.1587	0.8	1.8	3.5805	1.668	0.25608	2.0	6.65	1.9869	5
(28)	0.1584	0.6	1.7	3.5351	1.6826	0.25427	0.25	5.25	1.9773	5
(29)	0.1584	6.2	0.95	3.5357	1.6824	0.25427	2.25	0.85	1.9773	5
(30)	0.1252	0.15	0.6	4.3444	1.1429	0.25033	0.35	0.9	1.9565	5
(31)	0.1588	0.4	10	3.6463	1.646	0.2637	0.5	10	2.0279	5
(32)	0.1584	6.2	0.95	3.5357	1.6824	0.25427	2.55	0.85	1.9773	5

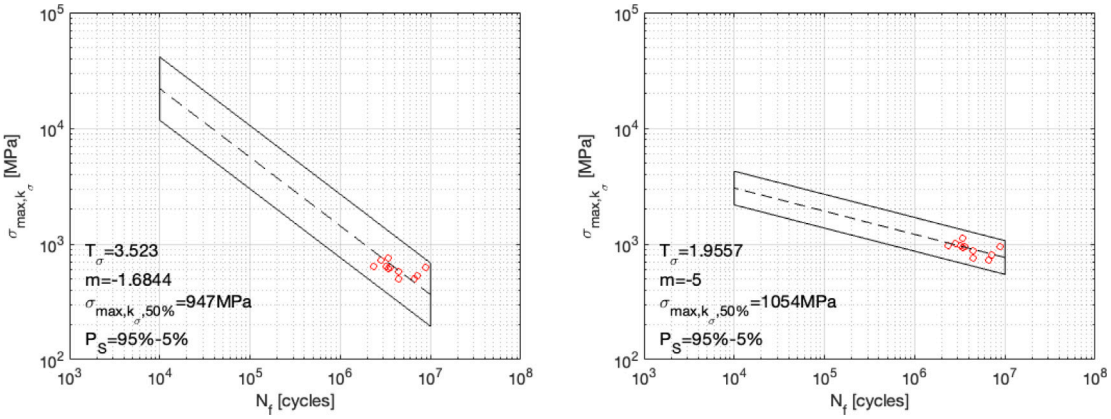

(a) *Free slope with* $\beta = 0.221$ *and* $\gamma = 0.653$ **(b)** *Fixed slope with* $\beta = 0.345$ *and* $\gamma = 0.895$

Fig. 10. Fatigue test results for the HFMI treated welds for actual geometry.

4.2.1. Analysis results for the actual geometry

The results of statistical analysis with the stress concentration factor from the actual model with the free and fixed slopes are tabulated Table 9.

Table 9 shows Eq. (30) results in the minimum σ_y standard deviation in which $\beta = 0.15$ and $\gamma = 0.6$. Subsequently, the different couples of β and γ values were used as a function of the standard deviation σ_y.

The minimum standard deviation evaluated for β and γ values were in between 0.05 and 1. Therefore another statistical analysis was done with a reduced interval of the two constant and also with a smaller step size, which resulted in $\sigma_y = 0.1582$, $\beta = 0.221$, $\gamma = 0.653$, $T_\sigma = 3.523$, $m = 1.6844$. Fig. 10(a) presents the analysis results for $\beta = 0.221$ and $\gamma = 0.653$ with a free slope for the fatigue test results obtained at VAL of R = −0.43 for HFMI-treated load-carrying transverse attachments. The analysis was repeated for the fixed slope of $m = 5$, which resulted in $\sigma_y = 0.2502$, $\beta = 0.345$, $\gamma = 0.895$, $T_\sigma = 1.9557$, see Fig. 10(b).

4.2.2. Analysis results for ENS approach

The statistical analyses results of the ENS approach for the reference model with angular misalignment are presented in Table 10 for free and fixed slopes.

As in the case of an actual model, Eq. (30) was resulted in the minimum σ_y standard deviation following the analyses of several couples of β and γ values. Thus, the values read $\sigma_y = 0.067973$, $\beta = 0.599$, $\gamma = 0.998$, $T_\sigma = 1.6768$, $m = 1.7628$ for a free slope and $\sigma_y = 0.18181$, $\beta = 0.391$, $\gamma = 0.966$, $T_\sigma = 1.6282$, for a fixed slope of $m = 5$.

The SN curves for $\beta = 0.599$ and $\gamma = 0.998$ with a free slope is represented in Fig. 11(a) and for $\beta = 0.391$ and $\gamma = 0.966$ with a fixed slope in Fig. 11(b).

4.2.3. Analysis results for PSM

The statistical analyses results of PSM on the reference model with angular misalignment are presented in Table 11 for free and fixed slopes.

Similar to the previous analyses, Eq. (30) was resulted in the minimum σ_y standard deviation following the analyses of several couples of β and γ values. Thus, the values are $\sigma_y = 0.071122$, $\beta = 0.599$, $\gamma = 0.998$, $T_\sigma = 1.7322$, $m = 1.7354$ for a free slope and $\sigma_y = 0.18845$, $\beta = 0.338$, $\gamma = 0.891$, $T_\sigma = 1.6574$ for a fixed slope of $m = 5$.

The SN curves for $\beta = 0.599$ and $\gamma = 0.998$ with a free slope is represented in Fig. 12(a) and for $\beta = 0.338$ and $\gamma = 0.891$ with a fixed slope in Fig. 12(b).

Table 10
Statistical analysis results for the ENS approach.

Equation for k_σ	*Free slope*					*Fixed slope*				
	σ_y	β	γ	T_σ	B (slope)	σ_y	β	γ	T_σ	B (slope)
(25)	0.12094	0.1	0.8	2.5171	1.7564	0.29553	0.1	7.55	2.1086	5
(26)	0.08968	0.2	9.1	1.608	2.5313	0.18597	0.2	6.45	1.6464	5
(27)	0.09031	0.75	4.35	1.6218	2.504	0.18764	1.1	8.2	1.6538	5
(28)	0.08984	0.75	1.5	1.6152	2.5118	0.18651	0.75	1.6	1.6488	5
(29)	0.08984	0.75	1.5	2.0618	2.5112	0.18651	6.85	0.95	1.6488	5
(30)	0.08865	0.3	0.85	1.5972	2.5383	0.18415	0.25	0.7	1.6384	5
(31)	0.09060	0.4	10	1.6285	2.4909	0.19047	0.5	10	1.6664	5
(32)	0.08984	0.85	0.7	1.6154	2.5112	0.18651	6.85	0.9	1.6464	5

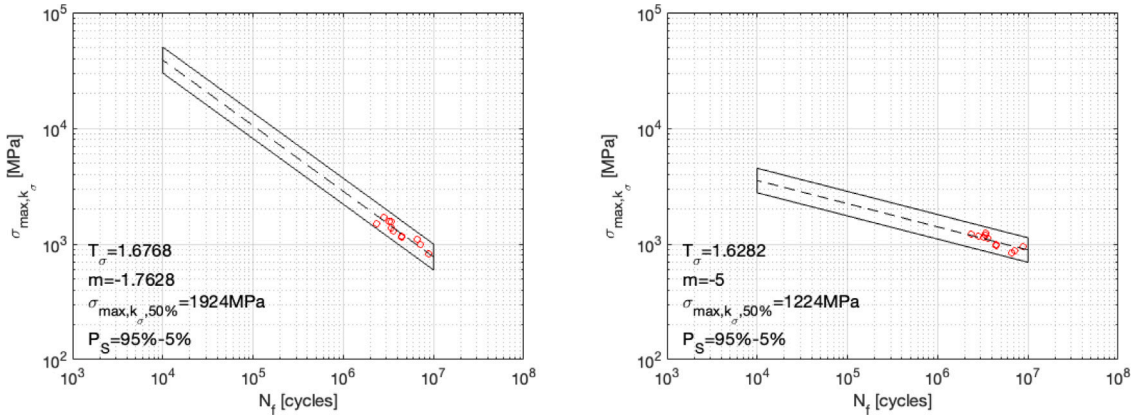

(a) *Free slope with* $\beta = 0.599$ *and* $\gamma = 0.998$ **(b)** *Fixed slope with for* $\beta = 0.391$ *and* $\gamma = 0.966$

Fig. 11. Fatigue test results of the HFMI treated welds with ENS.

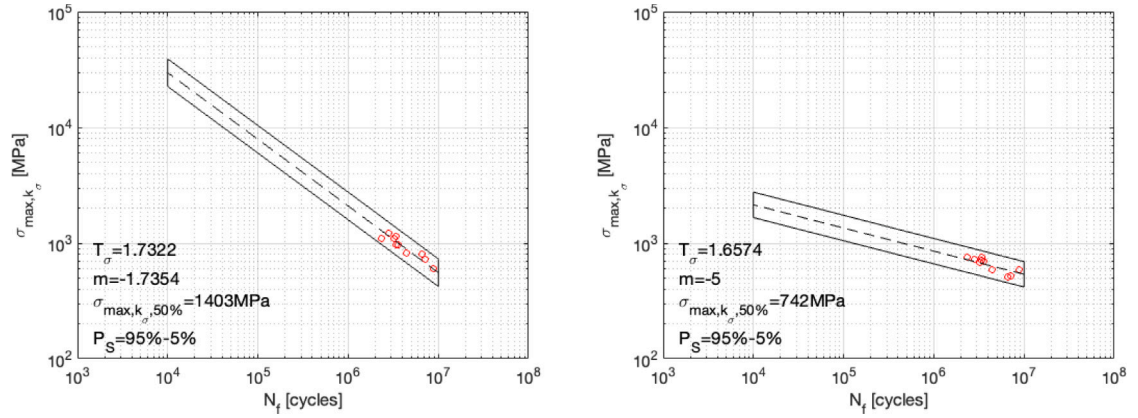

(a) *Free slope with* $\beta = 0.599$ *and* $\gamma = 0.998$ **(b)** *Fixed slope with for* $\beta = 0.338$ *and* $\gamma = 0.891$

Fig. 12. Fatigue test results of the HFMI treated welds with PSM.

Table 11
Statistical analysis results for the PSM.

Equation for k_σ	*Free slope*					*Fixed slope*				
	σ_y	β	γ	T_σ	B (slope)	σ_y	β	γ	T_σ	B (slope)
(25)	0.12554	0.1	1.5	2.7576	1.6591	0.31242	0.1	9.65	2.3109	5
(26)	0.09268	0.2	4.7	1.652	2.4752	0.19249	0.2	6.5	1.6755	5
(27)	0.09349	0.95	7.15	1.6638	2.4619	0.1922	1.55	9.5	1.6742	5
(28)	0.09301	6.9	1.05	1.6558	2.4725	0.19102	0.2	6.9	1.6689	5
(29)	0.09301	3.2	0.9	1.6557	2.4728	0.19103	0.2	6.9	1.6689	5
(30)	0.09236	0.25	0.7	1.6419	2.4971	0.18948	0.3	0.8	1.662	5
(31)	0.09431	0.45	10	1.6843	2.4251	0.1984	0.5	10	1.7022	5
(32)	0.09301	3.2	0.9	1.6557	2.4728	0.19103	7.55	0.95	1.6689	5

Table 12
Literature fatigue data points for welded joints based on the experiments at constant amplitude axial fatigue loading.

Ref.	Steel type	f_y [MPa]	Stress ratio R	Plate thickness [mm]	N° of data	Type of joints
[38]	S1100	≥1100	0.1	6	20	Butt Joints
[33]	S1100	≥1100	0.1	8	8	Cruciform joints
[16]	BS 4369 Grade 43A	347	0	12.5	41	Cruciform joints partial pen. and fillet welds
[21]	S690	690	0.1	5	27	T-joints
[19]	DH-36	355	−1	5	57	Cruciform Joints
[31]	RAEX S275	287	0	12	11	Butt Joints
[39]	Optim 1100QC	1100	0.05 /0.1 /0.57	6	20	Butt Joints
[40]	$15G_2ANb$	370	0.5/-1	8	41	Cruciform Joints
[41]	Fe510 D1	455	0	8	8	Butt Joints
[18]	ASTM A36	250	0	12	42	Butt Joints
[42]	RAEX S275	287	0	12	32	Butt Joints
[20]	S960 MC	960	0.1/0.2	8	4	T-joints
[17]	HW-50 HW-70	580 820	0.1	20	22	Butt Joints
[43]	A36	250	0	12.5 and 15.9	19	Butt Joints
[44]	BS4260 Grade 43A	275	0	12.5	22	Butt Joints
[45]	Damex 355 MC Damex 550 MC Weldax 960	355 550 960	0	12 3 3	72	Cruciform Joints

5. Extension for the literature data

5.1. Evaluation of k_σ based on the literature data

The objective has been to define a k_{mis} factor to determine the misalignment effect on the fatigue strength of welded joint tested at CAL. Thus a review of published experimental data was conducted on the fatigue strength of welded joints. The data included 16 publications containing fatigue data for as-welded steel joints with angular or axial misalignment that were subjected to Constant Amplitude Loading (CAL). The reported misalignment values and recommended local geometry parameters for the ENS and PSM methods. The analysis method was the same of that of described previously for the VAL data. Since the CAL data does not include real local weld geometry, analyses for actual geometry was not performed. The experimental data are summarised in Table 12. Full detailed results are provided in Appendix C.

5.2. Results comparison

The results of the statistical analysis with the k_σ function are presented in Tables 14–16.

In the case of ENS approach the minimum standard deviation was obtained by the proposed Eq. (31) with $\beta = 1.342$ and $\gamma = 1.266$ for the free slope and $\beta = 1.224$ and $\gamma = 1.374$ for the fixed slope of 3 [3]. On the other hand, Eq. (30) resulted in the minimum standard deviation for the analyses by PSM, where $\beta = 0.659$ and $\gamma = 0.996$ for the free slope, and $\beta = 0.630$ and $\gamma = 0.975$ for the fixed slope of 3, see Table 13.

As Tables 14–16 show, the use of k_σ function decreases the value of the standard deviation and the scatter band. Furthermore, the expression of k_σ function when the stress concentration factors obtained by the application of the ENS approach is the same for the free and fixed slope, i.e., the value of two constant β and γ that are roughly the same. The same consideration can be done for the k_σ function when the stress intensity factor obtained by the application of the PSM approach. Four SN curves are presented in Figs. 13–16 for comparison of the reduced scatter.

Table 13
Comparison of the ENS results with free slope.

ENS (Free slope)				
Without k_σ		*With* k_σ		*Δ%*
T_σ	23.7531	T_σ	3.0504	−87.16%
σ_y	0.5575	σ_y	0.36615	−34.32%

Table 14
Comparison of the ENS results with fixed slope.

ENS (Fixed slope m = 3)				
Without k_σ		*With* k_σ		*Δ%*
T_σ	6.0817	T_σ	2.6295	−56.76%
σ_y	0.7149	σ_y	0.38286	−46.45%

Table 15
Comparison of the PSM results with free slope.

PSM (Free slope)				
Without k_σ		*With* k_σ		*Δ%*
T_σ	22.1688	T_σ	3.0143	−86.40%
σ_y	0.5582	σ_y	0.36985	−33.74%

Table 16
Comparison of the PSM results with fixed slope.

PSM (Fixed slope m = 3)				
Without k_σ		*With* k_σ		*Δ%*
T_σ	5.9759	T_σ	2.6282	−56.02%
σ_y	0.7080	σ_y	0.38267	−45.95%

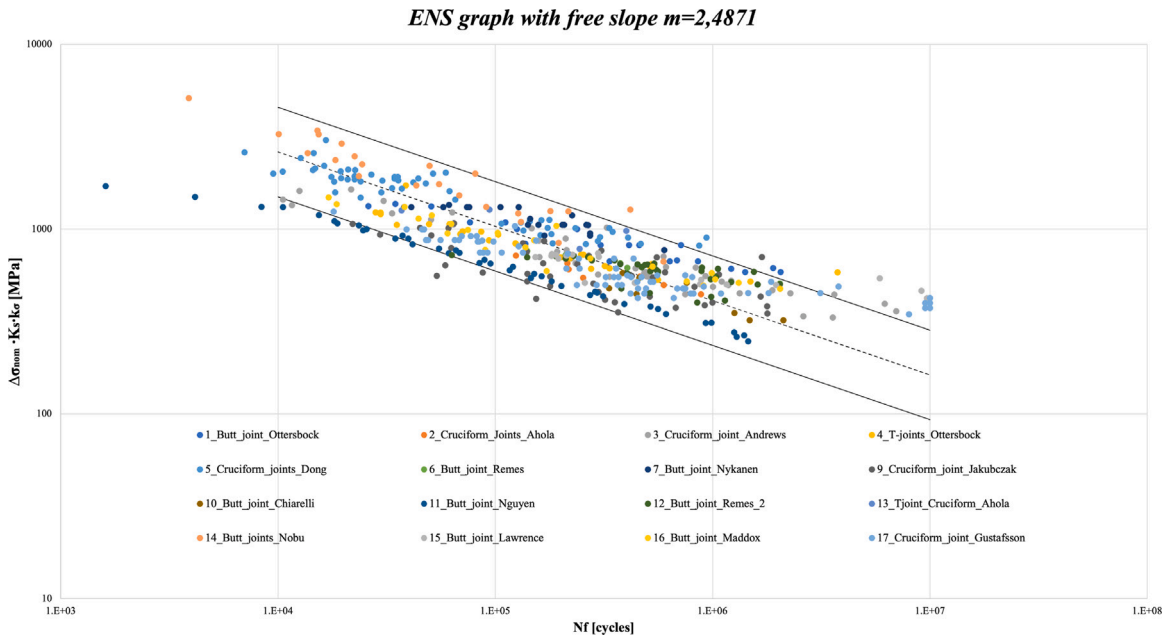

Fig. 13. SN curve in ENS approach for $\beta = 1.342$ and $\gamma = 1.266$ with the free slope.

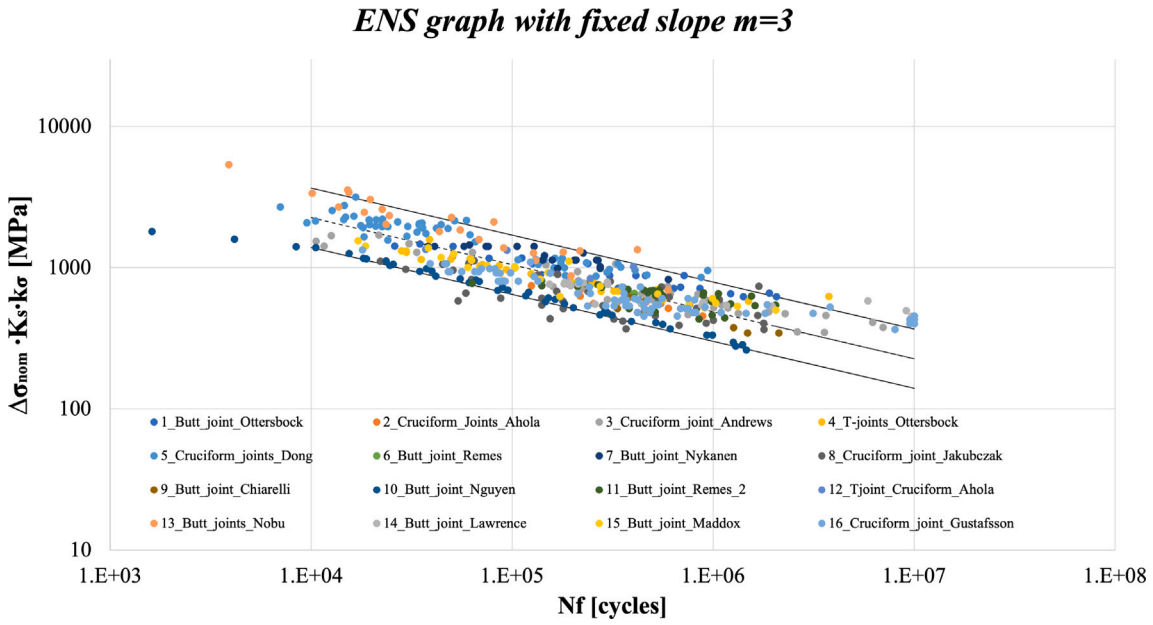

Fig. 14. SN curve in ENS approach for $\beta = 1.224$ and $\gamma = 1.374$ with the fixed slope.

6. Conclusions

The present work looked into the effect of the misalignment on the fatigue behaviour of welded steel joints. Two fatigue test results were included; experimental results for the HFMI treated load carrying transverse specimens tested at Variable Amplitude Loading (VAL) R = −0.43, and literature fatigue data for cruciform and butt joints tested at Constant Amplitude Loading (CAL). All the reported fatigue test results were conducted in axial loading.

In the case of CAL condition four SN curve were presented for the Effective Notch Stress approach and Peak Stress Method to consider the misalignment effect through the deriving k_σ, that is a function of the thickness and the existing joint misalignment. The scatter band of these curves were obtained through a statistical analysis with the objective to minimise the standard deviation and the ratio T_σ. This method applied with an imposed slope of $m = 3$, suggested slope to assess the weld fatigue in the as-welded condition, and also for the free slope per data set.

The resultant k_σ values following evaluations on the fatigue data for constant amplitude loading are summarised in Table 17. First observation is that all the ENS values are bigger than that of obtained from PSM, regardless of the slope. Second, the relative error in between cruciform and T-joints are quite less in the case of PSM when compared to ENS approach. This could be related to the nature of PSM, that is the method is calibrated to obtain equivalent stress values.

The used expression of the k_σ in the case of the application with ENS approach, can be used but it has to be verified by the IIW

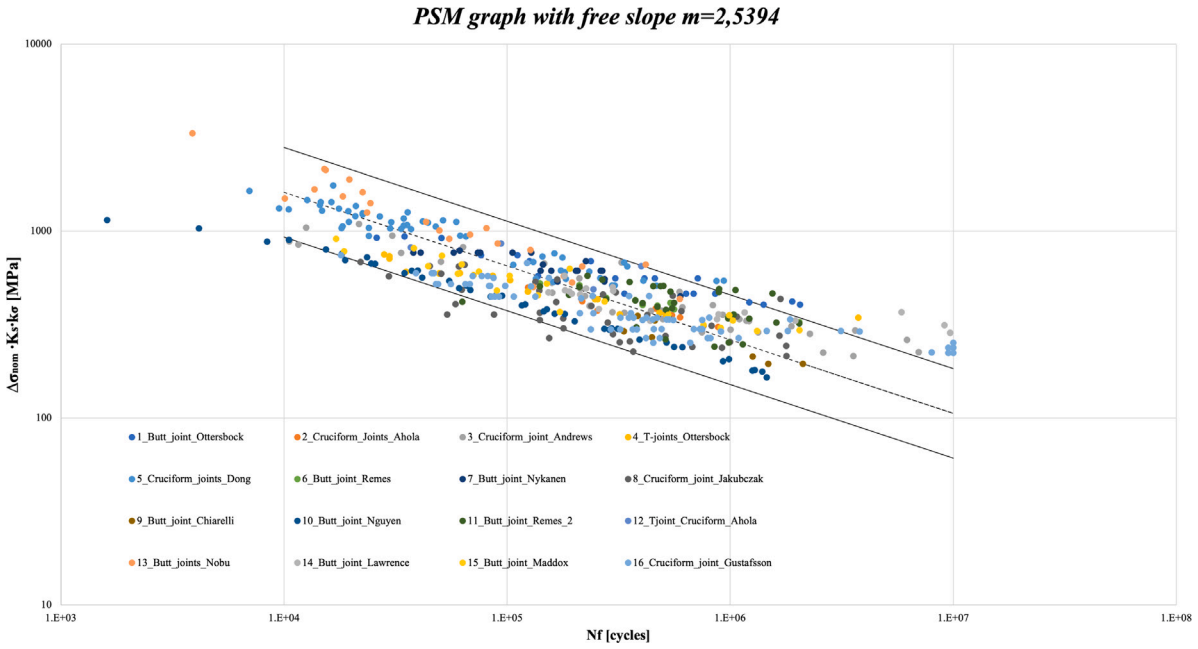

Fig. 15. SN curve in PSM for $\beta = 0.659$ and $\gamma = 0.996$ with the free slope.

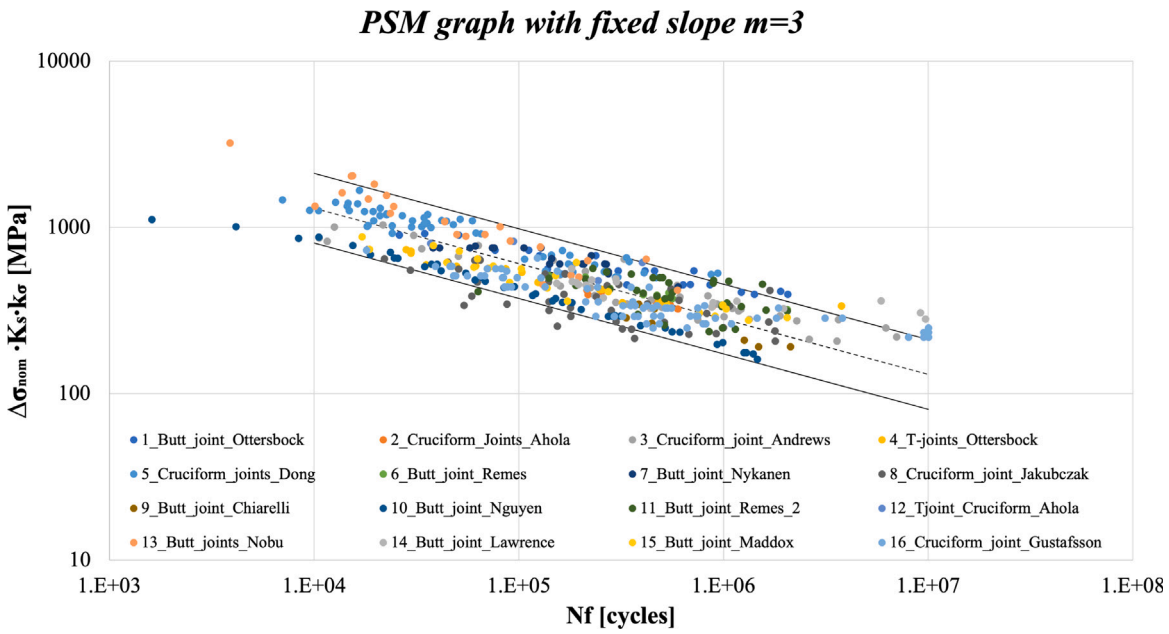

Fig. 16. SN curve in PSM for $\beta = 0.630$ and $\gamma = 0.975$ with the fixed slope.

Table 17
Results of k_σ for the cruciform and T-joint.

Cruciform Joint			
$k_{\sigma,PSM,free}$	$k_{\sigma,PSM,fixed}$	$k_{\sigma,ENS,free}$	$k_{\sigma,ENS,fixed}$
0.9954	0.9715	1.2053	1.2921
T-Joint			
0.9952	0.9704	1.1929	1.2750

Guidelines [15] for the fatigue behaviour assessment of steel welded joint in as-welded condition and subjected to an axial load.

In the case of HFMI treated welds at VAL, four SN curves were presented based on the Effective Notch Stress approach and Peak Stress Method to consider the misalignment effect by defining k_σ factors. The scatter band were obtained through the statistical analysis with the objective of minimising the standard deviation and the scatter band T_σ. This method has been applied with an fixed slope $m = 5$ and also for the free slope per data set.

Additionally, six factors were evaluated based on the FE models with and without angular misalignment. The factors help compare the real geometry results and the corresponding reference geometry to determine the misalignment effect and to understand the advantages of HFMI treatment for experimental data obtained at VAL.

In the derivation of the analytical k_σ, we hypothesised that the calibration for the scatter takes into account the several different features based on the data. That is, set by set, it accounts for the HFMI treatment and other well know variations for the experiments, e.g., different test setups and weld quality.

Relevant work is suggested for future developments:

Table A.18
Dimension of the samples.

Specimen	L [mm]	t [mm]	b [mm]	z [mm]	h [mm]	2α[°]	Right misalignment α_R [°]	Left misalignment α_L [°]
355-WH-2	600	6	6	6	33	135	1.16	1.48
355-WH-3	600	6	6	6.8	32	135	1.03	1.42
355-WH-4	600	6	6	5.8	33	135	0.91	1.32
355-WH-5	600	6	6	6	34	135	0.87	1.27
355-WH-8	600	6	6	6.8	33	135	0.64	1.25
355-WH-11	600	6	6	6.41	33	135	0.76	1.09
355-WH-14	600	6	6	6.5	33	135	1.03	1.51
355-WH-16	600	6	6	6.45	33	135	0.78	1.29
355-WH-17	600	6	6	6.45	33	135	0.80	1.23
355-WH-18	600	6	6	7	32.6	135	0.86	1.24
355-WH-20	600	6	6	6.2	34	135	0.86	1.07
355-WH-21	600	6	6	6.2	34	135	0.96	1.01
355-WH-22	600	6	6	7	33	135	1.01	0.94

1. The procedure to determine the k_σ should be verified by using other loading types for the HFMI welds as the stress relaxation and the misalignment would have coupling effect of the weld fatigue.
2. The FE analysis for the application of ENS and PSM should be improved with the imposition of displacement to simulate the action of the clamps when the specimen is inserted in the test machine;
3. The definition of the k_σ factor in VAL condition should be verified and compared with the experimental results. Thus, the same experimental procedure executed for CAL condition can be applied.

CRediT authorship contribution statement

Marco Soligo: Investigation, Data curation, Software, Formal analysis, Writing – original draft. **Alberto Campagnolo:** Supervision. **Giovanni Meneghetti:** Supervision. **Halid Can Yıldırım:** Writing – review & editing, Supervision.

Declaration of competing interest

The authors declare that they have no known competing financial interests or personal relationships that could have appeared to influence the work reported in this paper.

Data availability

No data was used for the research described in the article.

Appendix A. Local approach results for the experimental data at VAL

A.1. Geometry definitions

See Figs. A.17 and A.18 and Table A.18.

A.2. Local approach results

A.2.1. SHSS results for reference model

See Table A.19.

A.2.2. ENS results for reference model

See Table A.20.

Table A.19
SHSS results of reference model.

Specimen	$SHSS_{LSE,typeA}$ [MPa]	$SHSS_{LSE,typeB}$ [MPa]
355-WH-2	0.994	0.950
355-WH-3	0.992	0.948
355-WH-4	0.990	0.950
355-WH-5	0.994	0.950
355-WH-8	0.992	0.948
355-WH-11	0.993	0.949
355-WH-14	0.993	0.948
355-WH-16	0.993	0.949
355-WH-17	0.993	0.949
355-WH-18	0.992	0.947
355-WH-20	0.994	0.949
355-WH-21	0.994	0.949
355-WH-22	0.950	0.947

A.3. PSM results of reference model with sharp V-notch

See Table A.21.

A.4. PSM results of reference model with HFMI groove

See Table A.22.

A.4.1. SHSS results with angular misalignment

See Table A.23.

A.4.2. ENS results with angular misalignment

See Table A.24.

A.4.3. PSM results for angular misalignment with sharp V-notch

See Table A.25.

A.4.4. PSM results for angular misalignment with HFMI groove

See Table A.26.

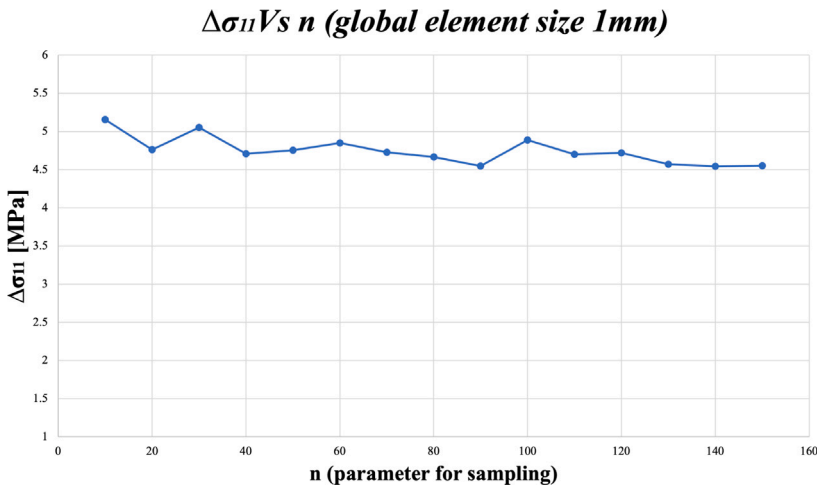

Fig. A.17. Graph to understand the influence of sampling parameter.

Table A.20
ENS results of reference model.

Specimen	$\Delta\sigma_{11,max,toe,ENS183}$ [MPa]	$\Delta\sigma_{11,max,root,ENS183}$ [MPa]	$\Delta\sigma_{11,max,toe,ENS182}$ [MPa]	$\Delta\sigma_{11,max,root,ENS182}$ [MPa]
355-WH-2	2.762	3.032	2.778	3.046
355-WH-3	2.564	2.756	2.576	2.768
355-WH-4	2.826	3.111	2.84	3.124
355-WH-5	2.761	3.032	2.777	3.046
355-WH-8	2.565	2.756	2.576	2.768
355-WH-11	2.65	2.883	2.664	2.897
355-WH-14	2.629	2.853	2.642	2.866
355-WH-16	2.64	2.87	2.653	2.882
355-WH-17	2.64	2.87	2.653	2.882
355-WH-18	2.527	2.695	2.538	2.707
355-WH-20	2.703	2.958	2.719	2.971
355-WH-21	2.703	2.958	2.719	2.971
355-WH-22	2.527	2.695	2.538	2.706

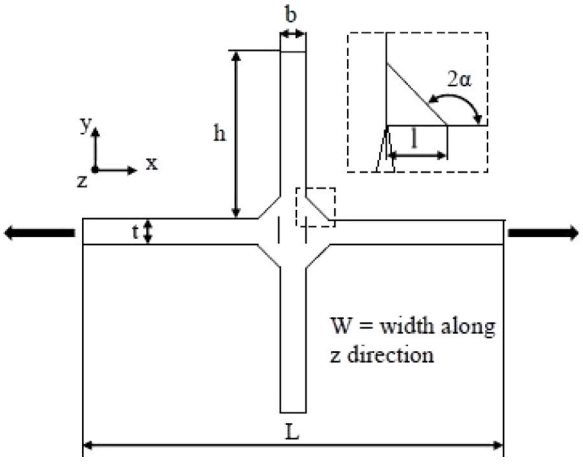

Fig. A.18. Definition of the principal dimension of the samples.

Table A.21
PSM results of reference model with sharp V-notch.

Specimen	$\sigma_{eq,peak,toe}$ [MPa]	$\sigma_{eq,peak,root}$ [MPa]
355-WH-2	1.946	1.945
355-WH-3	1.850	1.768
355-WH-4	1.977	1.994
355-WH-5	1.944	1.946
355-WH-8	1.851	1.771
355-WH-11	1.892	1.844
355-WH-14	1.878	1.834
355-WH-16	1.886	1.844
355-WH-17	1.886	1.844
355-WH-18	1.831	1.731
355-WH-20	1.917	1.898
355-WH-21	1.917	1.898
355-WH-22	1.831	1.731

Appendix B. Misalignment factors

B.1. Factors

B.1.1. Factor 1

See Table B.27.

B.1.2. Factor 2

See Table B.28.

B.1.3. Factor 3

See Table B.29.

B.1.4. Factor 4

See Table B.30.

Table A.22
PSM results of reference model with HFMI groove.

Specimen	$\sigma_{eq,peak,toe}$ [MPa]	$\sigma_{eq,peak,root}$ [MPa]
355-WH-2	1.685	2.028
355-WH-3	1.607	1.831
355-WH-4	1.699	2.08
355-WH-5	1.685	2.027
355-WH-8	1.607	1.821
355-WH-11	1.635	1.971
355-WH-14	1.630	1.932
355-WH-16	1.631	1.964
355-WH-17	1.631	1.964
355-WH-18	1.597	1.817
355-WH-20	1.652	1.974
355-WH-21	1.652	1.974
355-WH-22	1.596	1.792

Table A.23
SHSS results with angular misalignment.

Specimen	$SHSS_{LSE,typeA}$ [MPa]	$SHSS_{LSE,typeB}$ [MPa]
355-WH-2	3.227	3.177
355-WH-3	3.064	3.015
355-WH-4	2.892	2.844
355-WH-5	2.814	2.766
355-WH-8	2.614	2.568
355-WH-11	2.562	2.516
355-WH-14	3.149	3.100
355-WH-16	2.759	2.712
355-WH-17	2.720	2.673
355-WH-18	2.769	2.722
355-WH-20	2.622	2.575
355-WH-21	2.644	2.597
355-WH-22	2.620	2.573

Table A.24
ENS results with misalignment.

Specimen	$\Delta\sigma_{11,max,toe,ENS182}$ [MPa]	$\Delta\sigma_{11,max,root,ENS182}$ [MPa]	$\Delta\sigma_{11,max,toe,ENS183}$ [MPa]	$\Delta\sigma_{11,max,root,ENS183}$ [MPa]
355-WH-2	6.476	3.955	6.456	3.937
355-WH-3	6.000	3.445	5.979	3.428
355-WH-4	5.975	3.934	5.953	3.894
355-WH-5	5.776	3.776	5.755	3.758
355-WH-8	5.239	3.284	5.224	3.269
355-WH-11	5.236	3.455	5.221	3.442
355-WH-14	6.209	3.628	6.190	3.606
355-WH-16	5.561	3.506	5.542	3.491
355-WH-17	5.495	3.493	5.475	3.478
355-WH-18	5.462	3.253	5.447	3.238
355-WH-20	5.393	3.590	5.373	3.577
355-WH-21	5.427	3.604	5.409	3.590
355-WH-22	5.216	3.211	5.193	3.200

Table A.25
PSM results for angular misalignment with sharp V-notch.

Specimen	$\sigma_{eq,peak,toe}$ [MPa]	$\sigma_{eq,peak,root}$ [MPa]
355-WH-2	4.854	2.249
355-WH-3	4.573	1.981
355-WH-4	4.512	2.243
355-WH-5	4.321	2.161
355-WH-8	3.963	1.900
355-WH-11	3.940	1.988
355-WH-14	4.672	2.063
355-WH-16	4.174	2.002
355-WH-17	4.124	2.010
355-WH-18	4.145	1.881
355-WH-20	4.017	2.056
355-WH-21	4.041	2.062
355-WH-22	3.913	1.854

B.1.5. Factor 5

See Table B.31.

B.1.6. Factor 6

See Table B.32.

Table A.26
PSM results for angular misalignment with HFMI groove.

Specimen	$\sigma_{eq,peak,toe}$ [MPa]	$\sigma_{eq,peak,root}$ [MPa]
355-WH-2	4.708	2.354
355-WH-3	4.434	2.060
355-WH-4	4.216	2.357
355-WH-5	4.122	2.261
355-WH-8	3.793	1.951
355-WH-11	3.732	2.066
355-WH-14	4.569	2.161
355-WH-16	4.013	2.094
355-WH-17	3.950	2.099
355-WH-18	4.043	1.941
355-WH-20	3.836	2.141
355-WH-21	3.858	2.145
355-WH-22	3.801	1.913

Table B.27
Factor 1.

Specimen	$\Delta\sigma_{max,eq,peak,between-root\ and-toe-with-Misalignment}$ [MPa]	$\Delta\sigma_{max,eq,peak,between-root\ and-toe-without-Misalignment}$ [MPa]	$Factor_1$
355-WH-2	4.708	2.028	2.322
355-WH-3	4.434	1.831	2.422
355-WH-4	4.216	2.080	2.027
355-WH-5	4.122	2.027	2.033
355-WH-8	3.793	1.821	2.082
355-WH-11	3.732	1.971	1.894
355-WH-14	4.569	1.932	2.365
355-WH-16	4.013	1.964	2.044
355-WH-17	3.950	1.964	2.011
355-WH-18	4.043	1.817	2.225
355-WH-20	3.836	1.974	1.944
355-WH-21	3.858	1.974	1.955
355-WH-22	3.801	1.792	2.121

Table B.28
Factor 2.

Specimen	$\Delta\sigma_{11,max,toe-with-Misalignment,\ PLANE182}$ [MPa]	$\Delta\sigma_{11,max,toe-without-Misalignment,\ PLANE182}$ [MPa]	$Factor_2$
355-WH-2	6.476	2.778	2.331
355-WH-3	6.000	2.576	2.329
355-WH-4	5.975	2.840	2.104
355-WH-5	5.776	2.777	2.080
355-WH-8	5.239	2.576	2.034
355-WH-11	5.236	2.664	1.966
355-WH-14	6.209	2.642	2.350
355-WH-16	5.561	2.653	2.096
355-WH-17	5.495	2.653	2.071
355-WH-18	5.462	2.538	2.152
355-WH-20	5.393	2.719	1.984
355-WH-21	5.427	2.719	1.996
355-WH-22	5.216	2.538	2.055

Table B.29
Factor 3.

Specimen	$\Delta\sigma_{11,max,toe-with-Misalignment,\ PLANE183}$ [MPa]	$\Delta\sigma_{11,max,toe-without-Misalignment,\ PLANE183}$ [MPa]	$Factor_3$
355-WH-2	6.456	2.762	2.338
355-WH-3	5.979	2.564	2.332
355-WH-4	5.953	2.826	2.106
355-WH-5	5.755	2.761	2.085
355-WH-8	5.224	2.565	2.037
355-WH-11	5.221	2.650	1.970
355-WH-14	6.190	2.629	2.355
355-WH-16	5.542	2.640	2.099
355-WH-17	5.475	2.640	2.074
355-WH-18	5.447	2.527	2.155
355-WH-20	5.373	2.703	1.988
355-WH-21	5.409	2.703	2.001
355-WH-22	5.193	2.527	2.055

Table B.30
Results of factor 4.

Specimen	$SHSS_{LSE,with-Misalignment,type-A}$ [MPa]	$SHSS_{LSE,without-Misalignment,type-A}$ [MPa]	$Factor_4$
355-WH-2	3.227	0.994	3.245
355-WH-3	3.064	0.992	3.088
355-WH-4	2.892	0.990	2.920
355-WH-5	2.814	0.994	2.829
355-WH-8	2.614	0.992	2.635
355-WH-11	2.562	0.993	2.580
355-WH-14	3.149	0.993	3.171
355-WH-16	2.759	0.993	2.778
355-WH-17	2.720	0.993	2.739
355-WH-18	2.769	0.992	2.793
355-WH-20	2.622	0.994	2.639
355-WH-21	2.644	0.994	2.660
355-WH-22	2.620	0.992	2.642

Table B.31
Factor 5.

Specimen	$\Delta\sigma_{11,max,from-point-cloud\ with-Misalignment}$ [MPa]	$\Delta\sigma_{11,max,from-point-cloud\ without-Misalignment,PLANE182}$ [MPa]	$Factor_5$
355-WH-2	5.7937	2.778	2.086
355-WH-3	5.7993	2.576	2.251
355-WH-4	5.8974	2.840	2.077
355-WH-5	4.5343	2.777	1.633
355-WH-8	4.9200	2.576	1.910
355-WH-11	4.8354	2.664	1.815
355-WH-14	5.6188	2.642	2.127
355-WH-16	5.4915	2.653	2.070
355-WH-17	5.0055	2.653	1.887
355-WH-18	5.0221	2.538	1.979
355-WH-20	4.6786	2.719	1.721
355-WH-21	4.5449	2.719	1.672
355-WH-22	4.7214	2.538	1.860

Table B.32
Factor 6.

Specimen	$\Delta\sigma_{eq,peak,toe-with-Misalignment\ sharp-V-notch}$ [MPa]	$\Delta\sigma_{eq,peak,toe-with-Misalignment\ HFMI-groove}$ [MPa]	$Factor_6$
355-WH-2	4.854	4.708	1.031
355-WH-3	4.573	4.434	1.031
355-WH-4	4.512	4.216	1.070
355-WH-5	4.321	4.122	1.048
355-WH-8	3.963	3.793	1.045
355-WH-11	3.940	3.732	1.056
355-WH-14	4.672	4.569	1.023
355-WH-16	4.174	4.013	1.040
355-WH-17	4.124	3.950	1.044
355-WH-18	4.145	4.043	1.025
355-WH-20	4.017	3.836	1.047
355-WH-21	4.041	3.858	1.047
355-WH-22	3.913	3.801	1.029

Appendix C. Literature data for CAL

C.1. Results and experimental data from [38]

See Table C.33.

C.2. Results and experimental data from [33]

See Table C.34.

C.3. Results and experimental data from [16]

See Table C.35.

C.4. Results and experimental data from [21]

See Table C.36.

C.5. Results and experimental data from [19]

See Tables C.37 and C.38.

C.6. Results and experimental data from [31]

See Table C.39.

C.7. Results and experimental data from [39]

See Table C.40.

C.8. Results and experimental data from [40]

See Table C.41.

Table C.33
Experimental constant amplitude axial fatigue data for welded joints [38] and PSM and ENS results.

t [mm]	e [mm]	e/t	e_{tot} [mm]	α [°]	e from α [mm]	$\Delta\sigma_{nom}$ [MPa]	N_f [cycles]	K_{PSM} [MPa]	K_{ENS} [MPa]
6	0.75	0.125	0	0	0.75	503.01	34656	1.864	2.22782
6	0.75	0.125	0	0	0.75	399.83	76468	1.864	2.22782
6	0.75	0.125	0	0	0.75	399.91	111382	1.864	2.22782
6	0.75	0.125	0	0	0.75	300.32	305213	1.864	2.22782
6	0.75	0.125	0	0	0.75	300.37	412357	1.864	2.22782
6	0.75	0.125	0	0	0.75	300.44	459685	1.864	2.22782
6	0.75	0.125	0	0	0.75	248.45	685737	1.864	2.22782
6	0.75	0.125	0	0	0.75	300.44	715870	1.864	2.22782
6	0.75	0.125	0	0	0.75	223.62	1218111	1.864	2.22782
6	0.75	0.125	0	0	0.75	225.93	1897191	1.864	2.22782
6	1.5	0.25	0	0	1.5	400.49	26017	2.306	2.79286
6	1.5	0.25	0	0	1.5	399.33	50771	2.306	2.79286
6	1.5	0.25	0	0	1.5	300.44	125851	2.306	2.79286
6	1.5	0.25	0	0	1.5	250.10	137685	2.306	2.79286
6	1.5	0.25	0	0	1.5	300.57	237529	2.306	2.79286
6	1.5	0.25	0	0	1.5	200.84	335883	2.306	2.79286
6	1.5	0.25	0	0	1.5	200.93	633937	2.306	2.79286
6	1.5	0.25	0	0	1.5	201.01	856480	2.306	2.79286
6	1.5	0.25	0	0	1.5	175.66	1412010	2.306	2.79286
6	1.5	0.25	0	0	1.5	175.67	2056716	2.306	2.79286

Table C.34
Experimental constant amplitude axial fatigue data for welded joints [33] and PSM and ENS results.

t [mm]	e [mm]	e/t	e_{tot} [mm]	α [°]	e from α [mm]	$\Delta\sigma_{nom}$ [MPa]	N_f [cycles]	K_{PSM} [MPa]	K_{ENS} [MPa]
8	6	0.75	0	0	6.00	206	214769	2.123	2.81873
8	6	0.75	0	0	6.00	168	547795	2.123	2.81873
8	9	1.125	0	0	9.00	206	217244	2.074	2.68309
8	9	1.125	0	0	9.00	244	124297	2.074	2.68309
8	9	1.125	0	0	9.00	169	596207	2.074	2.68309
8	9	1.125	0	0	9.00	188	463560	2.074	2.68309
8	16	2	0	0	16.00	206	253715	1.799	2.48121
8	16	2	0	0	16.00	168	883148	1.799	2.48121

Table C.35
Experimental constant amplitude axial fatigue data for welded joints [16] and PSM and ENS results.

t [mm]	e [mm]	e/t	e_{tot} [mm]	α [°]	e from α [mm]	$\Delta\sigma_{nom}$ [MPa]	N_f [cycles]	K_{PSM} [MPa]	K_{ENS} [MPa]
12.5	3.125	0.25	0	0	3.125	142.59	192516	3.243	4.45172
12.5	3.125	0.25	0	0	3.125	122.88	233970	3.243	4.45172
12.5	3.125	0.25	0	0	3.125	91.85	1004330	3.243	4.45172
12.5	6.25	0.5	0	0	6.25	114.44	212919	4.321	5.83969
12.5	6.25	0.5	0	0	6.25	87.22	493070	4.321	5.83969
12.5	6.25	0.5	0	0	6.25	82.82	926731	4.321	5.83969
12.5	6.25	0.5	0	0	6.25	66.9	1333205	4.321	5.83969
12.5	9.375	0.75	0	0	9.375	85.54	223484	5.289	7.21842
12.5	9.375	0.75	0	0	9.38	70	296799	5.289	7.21842
12.5	9.375	0.75	0	0	9.38	54.75	747473	5.289	7.21842
12.5	9.375	0.75	0	0	9.38	40.92	3569802	5.289	7.21842
12.5	12.5	1	0	0	12.50	74.2	159327	6.378	8.61132
12.5	12.5	1	0	0	12.50	58.03	335894	6.378	8.61132
12.5	12.5	1	0	0	12.50	49.05	1883456	6.378	8.61132
12.5	12.5	1	0	0	12.50	35.5	2613788	6.378	8.61132
12.5	12.5	1	0	0	12.50	41.45	6195096	6.378	8.61132
12.5	3.125	0.25	0	0	3.13	221.92	10546	3.984	5.46003
12.5	3.125	0.25	0	0	3.13	172.78	50566	3.984	5.46003
12.5	3.125	0.25	0	0	3.13	132.98	158660	3.984	5.46003
12.5	3.125	0.25	0	0	3.13	94.26	441328	3.984	5.46003
12.5	3.125	0.25	0	0	3.125	84.95	498642	3.984	5.46003
12.5	6.25	0.5	0	0	6.25	153.07	33457	5.024	6.911761
12.5	6.25	0.5	0	0	6.25	132.83	63934	5.024	6.911761
12.5	6.25	0.5	0	0	6.25	111.62	210834	5.024	6.911761
12.5	6.25	0.5	0	0	6.25	72.86	484413	5.024	6.911761
12.5	6.25	0.5	0	0	6.25	78.26	610690	5.024	6.911761
12.5	6.25	0.5	0	0	6.25	169.66	11576	5.024	6.911761
12.5	6.25	0.5	0	0	6.25	66.08	1215377	5.024	6.911761
12.5	6.25	0.5	0	0	6.25	56.41	2276374	5.024	6.911761
12.5	6.25	0.5	0	0	6.25	45.11	6997402	5.024	6.911761
12.5	9.375	0.75	0	0	9.375	171.55	12549	6.125	8.34399

(*continued on next page*)

C.9. Results and experimental data from [41]

See Table C.42.

C.10. Results and experimental data from [18]

See Table C.43.

Table C.35 (*continued*).

t [mm]	e [mm]	e/t	e_{tot} [mm]	α [°]	e from α [mm]	$\Delta\sigma_{nom}$ [MPa]	N_f [cycles]	K_{PSM} [MPa]	K_{ENS} [MPa]
12.5	9.375	0.75	0	0	9.375	66.05	836434	6.125	8.34399
12.5	9.375	0.75	0	0	9.375	55.44	1100322	6.125	8.34399
12.5	12.5	1	0	0	12.5	152.15	21673	7.237	9.74413
12.5	12.5	1	0	0	12.5	132	30590	7.237	9.74413
12.5	12.5	1	0	0	12.5	114.56	63374	7.237	9.74413
12.5	12.5	1	0	0	12.5	93.61	146796	7.237	9.74413
12.5	12.5	1	0	0	12.5	94.74	325959	7.237	9.74413
12.5	12.5	1	0	0	12.5	66.03	593349	7.237	9.74413
12.5	12.5	1	0	0	12.5	46.27	1182798	7.237	9.74413
12.5	12.5	1	0	0	12.5	41.07	3632513	7.237	9.74413

Table C.36
Experimental constant amplitude axial fatigue data for welded joints [21] and PSM and ENS results.

t [mm]	e [mm]	e/t	e_{tot} [mm]	α [°]	e from α [mm]	$\Delta\sigma_{nom}$ [MPa]	N_f [cycles]	K_{PSM} [MPa]	K_{ENS} [MPa]
5	1.07	0.213	0	0	1.066	300	247930	1.445	2.019
5	1.19	0.238	0	0	1.189	500	29639	1.474	2.059
5	0.80	0.160	0	0	0.800	250	3753730	1.380	1.923
5	1.07	0.213	0	0	1.066	300	254183	1.445	2.019
5	1.09	0.217	0	0	1.087	400	70625	1.454	2.026
5	0.76	0.152	0	0	0.759	400	103163	1.371	1.920
5	1.03	0.205	0	0	1.025	500	29676	1.431	2.006
5	1.07	0.213	0	0	1.066	400	86119	1.445	2.019
5	1.21	0.242	0	0	1.210	500	28103	1.507	2.066
5	0.02	0.004	0	0	0.021	500	49513	1.189	1.683
5	−0.14	−0.029	0	0	−0.144	400	124270	1.194	1.630
5	−0.06	−0.012	0	0	−0.062	300	319375	1.200	1.656
5	−0.04	−0.008	0	0	−0.041	500	35196	1.214	1.663
5	−0.10	−0.021	0	0	−0.103	400	123710	1.189	1.643
5	−0.08	−0.016	0	0	−0.082	300	514187	1.200	1.649
5	0.12	0.025	0	0	0.123	300	523098	1.228	1.716
5	0.04	0.008	0	0	0.041	500	61503	1.194	1.690
5	−2.359	−0.472	0	0	−2.359	300	560492	/	0.933
5	−1.579	−0.316	0	0	−1.579	400	199715	/	1.169
5	−2.605	−0.521	0	0	−2.605	500	68931	/	0.859
5	−2.687	−0.537	0	0	−2.687	500	70962	/	0.835
5	−1.620	−0.324	0	0	−1.620	350	335610	/	1.157
5	−1.846	−0.369	0	0	−1.846	400	220275	/	1.088
5	−1.846	−0.369	0	0	−1.846	300	1493630	/	1.088
5	−2.174	−0.435	0	0	−2.174	500	93505	/	0.989
5	−2.174	−0.435	0	0	−2.174	350	275958	/	0.989
5	−3.097	−0.619	0	0	−3.097	600	38765	/	0.711

Table C.37
Experimental constant amplitude axial fatigue data for welded joints [19] and PSM and ENS results.

t [mm]	e [mm]	e/t	e_{tot} [mm]	α [°]	e from α [mm]	$\Delta\sigma_{nom}$ [MPa]	N_f [cycles]	K_{PSM} [MPa]	K_{ENS} [MPa]
5	1	0.2	1.41	3.69	4.69	414	16600	4.272	6.596
5	0	0	0.65	1.70	1.70	414	18100	2.512	3.719
5	0.95	0.19	0.05	0.13	1.08	414	59100	2.711	4.076
5	0.65	0.13	0.72	1.89	2.54	414	22600	2.998	4.386
5	1.45	0.29	0.78	2.04	3.49	414	12700	3.562	5.190
5	0.65	0.13	2.27	5.95	6.60	414	7000	4.077	5.779
5	0.4	0.08	0.29	0.76	1.16	414	61600	2.287	3.239
5	0.95	0.19	1.71	4.48	5.43	207	177100	3.533	4.926
5	1	0.2	0.21	0.55	1.55	207	936200	2.632	3.6832
5	0.05	0.01	0.92	2.41	2.46	414	37119	2.480	3.477
5	1.05	0.21	0.99	2.59	3.64	414	10500	3.178	4.392
5	0.95	0.19	0.74	1.94	2.89	414	22512	2.980	4.091
5	0.6	0.12	1.72	4.50	5.10	414	17600	3.215	4.199
5	0.2	0.04	0.74	1.94	2.14	414	65300	2.269	3.004
5	0.35	0.07	1.24	3.25	3.60	207	261000	2.723	3.562
5	0.75	0.15	0.57	1.49	2.24	414	29892	2.505	3.296
5	1.4	0.28	1.13	2.96	4.36	414	9500	3.224	4.330
5	0.15	0.03	1.36	3.56	3.71	207	867700	2.627	3.504
5	1.55	0.31	1.56	4.09	5.64	207	143800	3.584	4.839
5	0.3	0.06	1.79	4.69	4.99	414	35800	3.076	4.014
5	1.55	0.31	0.69	1.81	3.36	414	22500	3.024	3.968
5	0.25	0.05	1.21	3.17	3.42	414	18300	2.574	3.380
5	1.55	0.31	0.91	2.38	3.93	207	345900	3.148	4.161
5	1.15	0.23	0.64	1.68	2.83	207	183300	2.697	3.541
5	1	0.2	0.19	0.50	1.50	414	24000	2.284	3.021

Table C.38
Experimental constant amplitude axial fatigue data for welded joints [19] and PSM and ENS results.

t [mm]	e [mm]	e/t	e_{tot} [mm]	α [°]	e from α [mm]	$\Delta\sigma_{nom}$ [MPa]	N_f [cycles]	K_{PSM} [MPa]	K_{ENS} [MPa]
10	0.6	0.06	0.46	1.20	1.80	414	14600	3.458	5.148
10	0	0	0.13	0.34	0.34	414	35600	2.613	3.6991
10	0.2	0.02	0.15	0.39	0.59	207	134700	2.697	3.810
10	0.4	0.04	0.12	0.31	0.71	414	51600	2.761	3.894
10	0.5	0.05	0.02	0.05	0.55	207	161000	2.585	3.602
10	0.1	0.01	0.26	0.68	0.78	207	303700	2.480	3.539
10	1.8	0.18	0.13	0.34	2.14	414	14800	3.117	4.291
10	0.6	0.06	1.74	4.56	5.16	414	16300	3.462	4.618
10	0.8	0.08	0.82	2.15	2.95	414	19400	3.093	4.195
10	0.3	0.03	1.92	5.03	5.33	207	131000	3.321	4.576
10	0.2	0.02	0.14	0.37	0.57	414	24000	2.517	3.521
10	0.4	0.4	1.78	4.66	8.66	414	21000	3.310	4.545
10	1.5	0.15	0.54	1.41	2.91	207	106600	3.194	4.375
10	0.5	0.05	0.18	0.47	0.97	414	44200	2.690	3.690
10	0.7	0.07	0.48	1.26	1.96	414	26900	2.906	3.953
10	0.2	0.02	0.5	1.31	1.51	414	34400	2.592	3.722
10	0.1	0.01	0.71	1.86	1.96	414	19500	2.713	3.790
10	0.9	0.09	0.6	1.57	2.47	207	174000	2.979	4.118
10	1.1	0.11	0.32	0.84	1.94	207	233700	2.940	4.058
10	0.4	0.04	0.26	0.68	1.08	414	47800	2.563	3.4745
10	0.3	0.03	1.98	5.19	5.49	414	14477	3.350	4.395
10	0	0	0.88	2.30	2.30	207	408200	2.633	3.630
10	1.1	0.11	0.36	0.94	2.04	414	34400	2.826	3.857
10	0.8	0.08	0.18	0.47	1.27	414	30200	2.707	3.616
10	0.1	0.01	0.36	0.94	1.04	207	296100	2.478	3.389
10	0.1	0.01	0.49	1.28	1.38	414	33500	2.490	3.306
10	0.1	0.01	0.78	2.04	2.14	207	467100	2.470	3.353
10	0.7	0.07	0.82	2.15	2.85	414	41900	2.731	3.644
10	1.1	0.11	0.78	2.04	3.14	414	20900	2.917	3.802
10	1.6	0.16	0.41	1.07	2.67	207	181300	2.924	3.819
10	0.4	0.04	2.22	5.81	6.21	207	335000	3.298	4.302
10	0.5	0.05	3.26	8.54	9.04	207	162800	3.702	4.857

Table C.39
Experimental constant amplitude axial fatigue data for welded joints [31] and PSM and ENS results.

t [mm]	e [mm]	e/t	e_{tot} [mm]	α [°]	e from α [mm]	$\Delta\sigma_{nom}$ [MPa]	N_f [cycles]	K_{PSM} [MPa]	K_{ENS} [MPa]
12	0.25	0.021	0.51	1.11	1.363	199	1037495	1.800	2.275
12	0.29	0.024	0.46	1.00	1.294	181	2041188	1.808	2.280
12	0.32	0.027	0.39	0.85	1.171	224	471601	1.787	2.268
12	0.24	0.020	0.41	0.89	1.134	249	277963	1.766	2.229
12	0.17	0.014	0.36	0.79	0.955	201	979349	1.736	2.168
12	0.03	0.003	0.38	0.83	0.859	252	376019	1.698	2.093
12	0.07	0.006	1.63	3.56	3.627	269	140088	1.960	2.390
12	0.12	0.010	1.52	3.32	3.437	263	210665	1.959	2.322
12	0.17	0.014	1.35	2.95	3.116	247	539280	1.680	2.194
12	0.12	0.010	1.15	2.51	2.629	229	404503	1.764	2.247
12	0.02	0.002	1.01	2.20	2.224	253	560784	1.514	1.911

Table C.40
Experimental constant amplitude axial fatigue data for welded joints [39] and PSM and ENS results.

t [mm]	e [mm]	e/t	e_{tot} [mm]	α [°]	e from α [mm]	$\Delta\sigma_{nom}$ [MPa]	N_f [cycles]	K_{PSM} [MPa]	K_{ENS} [MPa]
6	0.136	0.023	0.24	0.628	1	500	38016	1.5385	2.1552
6	0.136	0.023	0.24	0.628	1	500	57593	1.5385	2.1552
6	0.136	0.023	0.24	0.628	1	500	75725	1.5385	2.1552
6	0.136	0.023	0.24	0.628	1	400	141306	1.5385	2.1552
6	0.136	0.023	0.24	0.628	1	400	157878	1.5385	2.1552
6	0.136	0.023	0.24	0.628	1	399	267032	1.5385	2.1552
6	0.136	0.023	0.24	0.628	1	292	598080	1.5385	2.1552
6	0.136	0.023	0.24	0.628	1	500	40987	1.5385	2.1552
6	0.136	0.023	0.24	0.628	1	500	74000	1.5385	2.1552
6	0.136	0.023	0.24	0.628	1	500	105620	1.5385	2.1552
6	0.136	0.023	0.24	0.628	1	500	128174	1.5385	2.1552
6	0.136	0.0227	0.24	0.63	0.764	350	168112	1.5385	2.1552
6	0.136	0.0227	0.24	0.63	0.764	400	203678	1.5385	2.1552
6	0.136	0.0227	0.24	0.63	0.764	400	207136	1.5385	2.1552
6	0.136	0.0227	0.24	0.63	0.764	450	225330	1.5385	2.1552
6	0.136	0.0227	0.24	0.63	0.764	400	262538	1.5385	2.1552
6	0.136	0.0227	0.24	0.63	0.764	350	273018	1.5385	2.1552
6	0.136	0.0227	0.24	0.63	0.764	360	273227	1.5385	2.1552
6	0.136	0.0227	0.24	0.63	0.764	513	61200	1.5385	2.1552
6	0.136	0.0227	0.24	0.63	0.764	432	144580	1.5385	2.1552

Table C.41
Experimental constant amplitude axial fatigue data for welded joints [40] and PSM and ENS results.

t [mm]	e [mm]	e/t	e_{tot} [mm]	α [°]	e from α [mm]	$\Delta\sigma_{nom}$ [MPa]	N_f [cycles]	K_{PSM} [MPa]	K_{ENS} [MPa]
8	3	0.375	0	0	3	105	140321	3.486	4.651
8	3	0.375	0	0	3	102	424464	3.486	4.651
8	3	0.375	0	0	3	93	282371	3.486	4.651
8	3	0.375	0	0	3	90	825675	3.486	4.651
8	3	0.375	0	0	3	79	1661524	3.486	4.651
8	3	0.375	0	0	3	79	513275	3.486	4.651
8	3	0.375	0	0	3	74	997801	3.486	4.651
8	3	0.375	0	0	3	70	1780947	3.486	4.651
8	6	0.75	0	0	6	81	87363	4.465	6.418
8	6	0.75	0	0	6	77	178685	4.465	6.418
8	6	0.75	0	0	6	68	178911	4.465	6.418
8	6	0.75	0	0	6	63	298391	4.465	6.418
8	6	0.75	0	0	6	57	319751	4.465	6.418
8	6	0.75	0	0	6	54	919445	4.465	6.418
8	6	0.75	0	0	6	48	1787957	4.465	6.418
8	8	1	0	0	8	76	58738	5.408	7.571
8	8	1	0	0	8	67	53806	5.408	7.571
8	8	1	0	0	8	62	140224	5.408	7.571
8	8	1	0	0	8	50	154168	5.408	7.571
8	8	1	0	0	8	48	354824	5.408	7.571
8	8	1	0	0	8	42	367356	5.408	7.571
8	8	1	0	0	8	45	675948	5.408	7.571
8	3	0.375	0	0	3	186	60837	3.486	4.651
8	3	0.375	0	0	3	154	133974	3.486	4.651
8	3	0.375	0	0	3	138	139252	3.486	4.651
8	3	0.375	0	0	3	132	269111	3.486	4.651
8	3	0.375	0	0	3	107	603725	3.486	4.651
8	6	0.75	0	0	6	98	1682973	4.465	6.418
8	6	0.75	0	0	6	79	1070233	4.465	6.418
8	6	0.75	0	0	6	90	238555	4.465	6.418
8	6	0.75	0	0	6	109	62598	4.465	6.418
8	6	0.75	0	0	6	106	307115	4.465	6.418
8	6	0.75	0	0	6	149	64545	4.465	6.418
8	6	0.75	0	0	6	129	29496	4.465	6.418
8	8	1	0	0	8	128	22032	5.408	7.571
8	8	1	0	0	8	110	50672	5.408	7.571
8	8	1	0	0	8	103	167911	5.408	7.571
8	8	1	0	0	8	84	552900	5.408	7.571
8	8	1	0	0	8	78	165906	5.408	7.571
8	8	1	0	0	8	65	530106	5.408	7.571
8	8	1	0	0	8	121	44973	5.408	7.571

Table C.42
Experimental constant amplitude axial fatigue data for welded joints [41] and PSM and ENS results.

t [mm]	e [mm]	e/t	e_{tot} [mm]	α [°]	e from α [mm]	$\Delta\sigma_{nom}$ [MPa]	N_f [cycles]	K_{PSM} [MPa]	K_{ENS} [MPa]
8	1.2	0.15	0	0	1	176.68	385123	1.998	2.69184
8	1.2	0.15	0	0	1	146.11	333625	1.998	2.69184
8	1.2	0.15	0	0	1	135.94	445968	1.998	2.69184
8	1.2	0.15	0	0	1	166.51	459132	1.998	2.69184
8	1.2	0.15	0	0	1	156.21	759754	1.998	2.69184
8	1.2	0.15	0	0	1	107.20	1259943	1.998	2.69184
8	1.2	0.15	0	0	1	98.08	1479637	1.998	2.69184
8	1.2	0.15	0	0	1	98.05	2117314	1.998	2.69184

Table C.43
Experimental constant amplitude axial fatigue data for welded joints [18] and PSM and ENS results.

t [mm]	e [mm]	e/t	e_{tot} [mm]	α [°]	e from α [mm]	$\Delta\sigma_{nom}$ [MPa]	N_f [cycles]	K_{PSM} [MPa]	K_{ENS} [MPa]
12	1.2	0.1	0	0	1.20	339.83	18777	2.060	2.569
12	1.2	0.1	0	0	1.20	235.26	68417	2.060	2.569
12	1.2	0.1	0	0	1.20	197.59	120479	2.060	2.569
12	1.2	0.1	0	0	1.20	175.81	163191	2.060	2.569
12	1.2	0.1	0	0	1.20	144.78	287447	2.060	2.569
12	1.2	0.1	0	0	1.20	116.95	560059	2.060	2.569
12	1.2	0.1	0	0	1.20	98.19	928456	2.060	2.569
12	1.2	0.1	0	0	1.20	87.37	1257607	2.060	2.569
12	2.4	0.2	0	0	2.40	348.36	8391	2.524	3.143
12	2.4	0.2	0	0	2.40	243.86	37387	2.524	3.143
12	2.4	0.2	0	0	2.40	202.80	65846	2.524	3.143
12	2.4	0.2	0	0	2.40	180.45	89189	2.524	3.143
12	2.4	0.2	0	0	2.40	151.52	150861	2.524	3.143

(*continued on next page*)

Table C.43 (*continued*).

t [mm]	e [mm]	e/t	e_{tot} [mm]	α [°]	e from α [mm]	$\Delta\sigma_{nom}$ [MPa]	N_f [cycles]	K_{PSM} [MPa]	K_{ENS} [MPa]
12	2.4	0.2	0	0	2.40	120.01	294013	2.524	3.143
12	2.4	0.2	0	0	2.40	100.79	517745	2.524	3.143
12	2.4	0.2	0	0	2.40	82.22	988543	2.524	3.143
12	2.4	0.2	0	0	2.40	70.34	1394716	2.524	3.143
12	3.6	0.3	0	0	3.6	343.48	4149	3.021	3.684
12	3.6	0.3	0	0	3.6	240.79	23537	3.021	3.684
12	3.6	0.3	0	0	3.6	204.19	39807	3.021	3.684
12	3.6	0.3	0	0	3.6	179.93	55022	3.021	3.684
12	3.6	0.3	0	0	3.6	149.61	94973	3.021	3.684
12	3.6	0.3	0	0	3.6	119.66	181382	3.021	3.684
12	3.6	0.3	0	0	3.6	99.50	313082	3.021	3.684
12	3.6	0.3	0	0	3.6	79.59	610086	3.021	3.684
12	3.6	0.3	0	0	3.6	60.03	1289507	3.021	3.684
12	4.8	0.4	0	0	4.8	348.35	1611	3.297	4.213
12	4.8	0.4	0	0	4.8	242.56	15422	3.297	4.213
12	4.8	0.4	0	0	4.8	203.65	25566	3.297	4.213
12	4.8	0.4	0	0	4.8	181.21	34630	3.297	4.213
12	4.8	0.4	0	0	4.8	150.70	60989	3.297	4.213
12	4.8	0.4	0	0	4.8	121.72	116463	3.297	4.213
12	4.8	0.4	0	0	4.8	100.22	201052	3.297	4.213
12	4.8	0.4	0	0	4.8	80.17	391780	3.297	4.213
12	4.8	0.4	0	0	4.8	50.28	1458411	3.297	4.213
12	6	0.5	0	0	6	201.23	18161	3.766	4.774
12	6	0.5	0	0	6	179.06	24599	3.766	4.774
12	6	0.5	0	0	6	150.35	41608	3.766	4.774
12	6	0.5	0	0	6	119.11	84421	3.766	4.774
12	6	0.5	0	0	6	99.04	145719	3.766	4.774
12	6	0.5	0	0	6	79.99	272716	3.766	4.774
12	6	0.5	0	0	6	239.62	10523	3.766	4.774

Table C.44
Experimental constant amplitude axial fatigue data for welded joints [42] and PSM and ENS results.

t [mm]	e [mm]	e/t	e_{tot} [mm]	α [°]	e from α [mm]	$\Delta\sigma_{nom}$ [MPa]	N_f [cycles]	K_{PSM} [MPa]	K_{ENS} [MPa]
12	0.25	0.021	0.51	1.11	1.36	199	1037495	1.805	2.258
12	0.29	0.024	0.46	1.00	1.29	181	2041188	1.776	2.262
12	0.32	0.027	0.39	0.85	1.17	224	471601	1.763	2.252
12	0.24	0.020	0.41	0.89	1.13	249	277963	1.739	2.213
12	0.17	0.014	0.36	0.79	0.96	201	979349	1.701	2.152
12	0.14	0.012	0.4	0.87	1.01	269	189524	1.702	2.147
12	0.03	0.003	0.38	0.83	0.86	252	376019	1.693	2.074
12	0.02	0.002	0.43	0.94	0.96	200	1217355	1.706	2.089
12	0.13	0.011	0.38	0.83	0.96	224	516276	1.694	2.134
12	0.17	0.014	0.4	0.87	1.04	226	549004	1.713	2.168
12	0.25	0.021	0.38	0.83	1.08	184	1611693	1.763	2.207
12	0.31	0.008	0.38	0.83	1.14	201	513309	1.314	1.818
12	0.42	0.026	0.42	0.92	1.34	302	63011	1.392	1.951
12	0.3	0.035	0.48	1.05	1.35	190	984909	1.338	1.844
12	0.09	0.025	0.49	1.07	1.16	251	380053	1.222	1.544
12	0.19	0.008	0.2	0.44	0.63	201	849199	1.202	1.602
12	0.19	0.016	0.34	0.74	0.93	201	1138300	1.239	1.650
12	0.07	0.006	1.63	3.56	3.63	269	140088	1.885	2.211
12	0.12	0.010	1.52	3.32	3.44	263	210665	1.915	2.226
12	0.17	0.014	1.35	2.95	3.12	247	539280	1.928	2.216
12	0.12	0.010	1.15	2.51	2.63	229	404503	1.802	2.090
12	0.02	0.002	1.01	2.20	2.22	253	560784	1.639	1.936
12	0.43	0.036	0.42	0.92	1.35	252	354052	2.127	2.195
12	0.39	0.033	0.44	0.96	1.35	264	267320	2.088	2.178
12	0.43	0.036	0.35	0.76	1.19	242	451699	2.102	2.164
12	0.47	0.039	0.37	0.81	1.28	226	1057498	2.146	2.197
12	0.49	0.041	0.38	0.83	1.32	235	487091	2.166	2.214
12	0.51	0.043	0.36	0.79	1.30	218	888604	2.171	2.217
12	0.58	0.048	0.34	0.74	1.32	260	229253	2.223	2.250
12	0.47	0.039	0.34	0.74	1.21	239	502035	2.133	2.185
12	0.49	0.041	0.32	0.70	1.19	218	1546593	2.131	2.188
12	0.46	0.038	0.37	0.81	1.27	230	892600	2.137	2.191

C.11. Results and experimental data from [42]

See Table C.44.

C.12. Results and experimental data from [20]

See Table C.45.

C.13. Results and experimental data from [17]

See Table C.46.

C.14. Results and experimental data from [43]

See Table C.47.

Table C.45
Experimental constant amplitude axial fatigue data for welded joints [20] and PSM and ENS results.

t [mm]	e [mm]	e/t	e_{tot} [mm]	α [°]	e from α [mm]	$\Delta\sigma_{nom}$ [MPa]	N_f [cycles]	K_{PSM} [MPa]	K_{ENS} [MPa]
8	0	0	1.15	6.60	6.60	299	94000	2.892	3.817
8	0	0	1.39	7.99	7.99	210	400000	3.119	4.214
8	0	0	0.33	1.88	1.88	378	37000	2.171	2.797
8	0	0	0.18	1.02	1.02	248	244000	1.975	2.581

Table C.46
Experimental constant amplitude axial fatigue data for welded joints [17] and PSM and ENS results.

t [mm]	e [mm]	e/t	e_{tot} [mm]	α [°]	e from α [mm]	$\Delta\sigma_{nom}$ [MPa]	N_f [cycles]	K_{PSM} [MPa]	K_{ENS} [MPa]
20	10	0.5	0	0	10	288.56	80854	3.607	6.017
20	10	0.5	0	0	10	184.34	418307	3.607	6.017
20	15	0.75	0	0	15	698.07	3882	4.800	6.525
20	15	0.75	0	0	15	351.00	13677	4.800	6.525
20	15	0.75	0	0	15	321.69	18348	4.800	6.525
20	15	0.75	0	0	15	234.95	43322	4.800	6.525
20	15	0.75	0	0	15	165.92	127196	4.800	6.525
20	20	1 0	0	0	20	159.97	68262	6.040	8.611
20	20	1 0	0	0	20	88.62	195644	6.040	8.611
20	30	1.5	0	0	30	163.86	49755	8.705	12.405
20	30	1.5	0	0	30	93.50	179379	8.705	12.405
20	10	0.5	0	0	10	253.07	55076	3.607	6.017
20	10	0.5	0	0	10	180.29	216858	3.607	6.017
20	15	0.75	0	0	15	444.29	15369	4.800	6.525
20	15	0.75	0	0	15	396.14	19609	4.800	6.525
20	15	0.75	0	0	15	338.04	22527	4.800	6.525
20	15	0.75	0	0	15	263.91	23570	4.800	6.525
20	15	0.75	0	0	15	179.80	90653	4.800	6.525
20	15	0.75	0	0	15	90.99	594386	4.800	6.525
20	20	1 0	0	0	20	358.95	15175	6.040	8.611
20	20	1 0	0	0	20	235.80	24393	6.040	8.611
20	30	1.5	0	0	30	243.24	10081	8.705	12.405
20	30	1.5	0	0	30	243.24	10081	8.705	12.405

Table C.47
Experimental constant amplitude axial fatigue data for welded joints [43] and PSM and ENS results.

t [mm]	e [mm]	e/t	e_{tot} [mm]	α [°]	e from α [mm]	$\Delta\sigma_{nom}$ [MPa]	N_f [cycles]	K_{PSM} [MPa]	K_{ENS} [MPa]
12.5	0	0	0.57	1.78	1.78	227.5	181000	2.540	2.585
12.5	0	0	0.31	0.96	0.96	227.5	195000	2.040	2.458
12.5	0	0	0.63	1.96	1.96	227.5	226000	2.170	2.634
12.5	0	0	0.77	2.38	2.38	227.5	297000	2.206	2.693
12.5	0	0	0.54	1.67	1.67	227.5	299000	2.113	2.553
12.5	0	0	0.71	2.20	2.20	165.5	887000	2.176	2.654
12.5	0	0	0.69	2.13	2.13	131	9680000	2.191	2.662
12.5	0	0	0.77	2.38	2.38	144.8	9130000	2.171	2.653
12.5	0	0	0.25	0.78	0.78	165.5	1960000	2.007	2.425
12.5	0	0	0.26	0.82	0.82	165.5	874000	2.044	2.448
12.5	0	0	0.25	0.78	0.78	165.5	1160000	2.224	2.439
15.9	0	0	0.92	2.85	2.85	227.5	212300	2.021	2.615
15.9	0	0	0.08	0.25	0.25	227.5	153000	2.069	2.468
15.9	0	0	0.09	0.28	0.28	227.5	213000	2.017	2.521
15.9	0	0	0.26	0.82	0.82	227.5	190000	2.097	2.556
15.9	0	0	0.33	1.03	1.03	227.5	182000	2.121	2.591
15.9	0	0	0.21	0.64	0.64	165.5	258000	2.320	2.475
15.9	0	0	0.46	1.42	1.42	165.5	5868000	2.228	2.656
15.9	0	0	0.09	0.28	0.28	165.5	438000	2.008	2.463

Table C.48
Experimental constant amplitude axial fatigue data for welded joints [44] and PSM and ENS results.

t [mm]	e [mm]	e/t	e_{tot} [mm]	α [°]	e from α [mm]	$\Delta\sigma_{nom}$ [MPa]	N_f [cycles]	K_{PSM} [MPa]	K_{ENS} [MPa]
12.5	3.2	0.256	0	0	3.2	240	191100	2.630	3.645
12.5	3.2	0.256	0	0	3.2	220	102560	2.630	3.645
12.5	3.2	0.256	0	0	3.2	200	150700	2.630	3.645
12.5	3.2	0.256	0	0	3.2	160	273380	2.630	3.645
12.5	3.2	0.256	0	0	3.2	120	758960	2.630	3.645
12.5	6.3	0.504	0	0	6.3	200	51000	3.709	5.161
12.5	6.3	0.504	0	0	6.3	180	62650	3.709	5.161
12.5	6.3	0.504	0	0	6.3	160	60200	3.709	5.161

(*continued on next page*)

C.15. Results and experimental data from [44]

See Table C.48.

C.16. Results and experimental data from [45]

See Tables C.49 and C.50.

Table C.48 (*continued*).

t [mm]	e [mm]	e/t	e_{tot} [mm]	α [°]	e from α [mm]	$\Delta\sigma_{nom}$ [MPa]	N_f [cycles]	K_{PSM} [MPa]	K_{ENS} [MPa]
12.5	6.3	0.504	0	0	6.3	130	89900	3.709	5.161
12.5	6.3	0.504	0	0	6.3	100	172300	3.709	5.161
12.5	6.3	0.504	0	0	6.3	90	1028400	3.709	5.161
12.5	6.3	0.504	0	0	6.3	80	2045200	3.709	5.161
12.5	9.5	0.76	0	0	9.5	180	17100	5.090	7.350
12.5	9.5	0.76	0	0	9.5	160	38200	5.090	7.350
12.5	9.5	0.76	0	0	9.5	120	74800	5.090	7.350
12.5	9.5	0.76	0	0	9.5	70	990100	5.090	7.350
12.5	9.5	0.76	0	0	9.5	60	906500	5.090	7.350
12.5	12.5	1	0	0	12.5	120	18600	6.554	10.312
12.5	12.5	1	0	0	12.5	100	44300	6.554	10.312
12.5	12.5	1	0	0	12.5	70	137400	6.554	10.312
12.5	12.5	1	0	0	12.5	55	528300	6.554	10.312
12.5	12.5	1	0	0	12.5	45	1319000	6.554	10.312

Table C.49
Experimental constant amplitude axial fatigue data for welded joints [45] and PSM and ENS results.

t [mm]	e [mm]	e/t	e_{tot} [mm]	α [°]	e from α [mm]	$\Delta\sigma_{nom}$ [MPa]	N_f [cycles]	K_{PSM} [MPa]	K_{ENS} [MPa]
12	0	0	0.29	1.13	1.13	150	351000	2.304	2.975
12	0	0	0.29	1.13	1.13	130	731000	2.304	2.975
12	0	0	0.29	1.13	1.13	130	687000	2.304	2.975
12	0	0	0.29	1.13	1.13	220	128000	2.304	2.975
12	0	0	0.29	1.13	1.13	130	748000	2.304	2.975
12	0	0	0.29	1.13	1.13	250	77000	2.304	2.975
12	0	0	0.29	1.13	1.13	150	421000	2.304	2.975
12	0	0	0.29	1.13	1.13	150	322000	2.304	2.975
12	0	0	0.29	1.13	1.13	130	454000	2.304	2.975
12	0	0	0.29	1.13	1.13	250	70000	2.304	2.975
12	0	0	0.29	1.13	1.13	150	369000	2.304	2.975
12	0	0	0.29	1.13	1.13	130	493000	2.304	2.975
12	0	0	0.29	1.13	1.13	150	806000	2.304	2.975
12	0	0	0.29	1.13	1.13	150	471000	2.304	2.975
12	0	0	0.29	1.13	1.13	250	82000	2.304	2.975
3	0	0	0.95	1.50	1.50	300	123000	2.256	3.008
3	0	0	0.95	1.50	1.50	150	450000	2.256	3.008
3	0	0	0.95	1.50	1.50	100	8000000	2.256	3.008
3	0	0	0.95	1.50	1.50	250	87000	2.256	3.008
3	0	0	0.95	1.50	1.50	130	1456000	2.256	3.008
3	0	0	0.95	1.50	1.50	130	1810000	2.256	3.008
3	0	0	0.95	1.50	1.50	130	3131000	2.256	3.008
3	0	0	0.95	1.50	1.50	200	242000	2.256	3.008
3	0	0	0.95	1.50	1.50	150	518000	2.256	3.008
3	0	0	0.95	1.50	1.50	150	533000	2.256	3.008
3	0	0	0.95	1.50	1.50	150	1856000	2.256	3.008
3	0	0	0.95	1.50	1.50	200	352000	2.256	3.008
3	0	0	0.95	1.50	1.50	200	433000	2.256	3.008
3	0	0	0.95	1.50	1.50	250	154000	2.256	3.008

Table C.50
Experimental constant amplitude axial fatigue data for welded joints [45] and PSM and ENS results.

t [mm]	e [mm]	e/t	e_{tot} [mm]	α [°]	e from α [mm]	$\Delta\sigma_{nom}$ [MPa]	N_f [cycles]	K_{PSM} [MPa]	K_{ENS} [MPa]
3	0	0	0.17	0.26	0.26	200	909000	1.456	1.983
3	0	0	0.17	0.26	0.26	200	3800000	1.456	1.983
3	0	0	0.17	0.26	0.26	300	215000	1.456	1.983
3	0	0	0.17	0.26	0.26	230	748000	1.456	1.983
3	0	0	0.17	0.26	0.26	230	405000	1.456	1.983
3	0	0	0.17	0.26	0.26	230	556000	1.456	1.983
3	0	0	0.17	0.26	0.26	350	98000	1.456	1.983
3	0	0	0.17	0.26	0.26	350	83000	1.456	1.983
3	0	0	0.17	0.26	0.26	350	84000	1.456	1.983
3	0	0	0.17	0.26	0.26	250	212000	1.456	1.983
3	0	0	0.17	0.26	0.26	250	244000	1.456	1.983
3	0	0	0.17	0.26	0.26	250	359000	1.456	1.983
3	0	0	0.21	0.33	0.33	200	382000	1.492	2.028
3	0	0	0.21	0.33	0.33	150	10000000	1.492	2.028
3	0	0	0.21	0.33	0.33	300	134000	1.492	2.028
3	0	0	0.21	0.33	0.33	180	817000	1.492	2.028
3	0	0	0.21	0.33	0.33	180	1091000	1.492	2.028

(*continued on next page*)

Table C.50 (*continued*).

t [mm]	e [mm]	e/t	e_{tot} [mm]	α [°]	e from α [mm]	$\Delta\sigma_{nom}$ [MPa]	N_f [cycles]	K_{PSM} [MPa]	K_{ENS} [MPa]
3	0	0	0.21	0.33	0.33	180	484000	1.492	2.028
3	0	0	0.21	0.33	0.33	350	48000	1.492	2.028
3	0	0	0.21	0.33	0.33	200	237000	1.492	2.028
3	0	0	0.21	0.33	0.33	300	88000	1.492	2.028
3	0	0	0.21	0.33	0.33	350	49000	1.492	2.028
3	0	0	0.21	0.33	0.33	150	9500000	1.492	2.028
3	0	0	0.21	0.33	0.33	350	65000	1.492	2.028
3	0	0	0.21	0.33	0.33	500	18000	1.492	2.028
3	0	0	0.21	0.33	0.33	200	292000	1.492	2.028
3	0	0	0.21	0.33	0.33	300	107000	1.492	2.028
3	0	0	0.21	0.33	0.33	300	92000	1.492	2.028
3	0	0	0.21	0.33	0.33	200	366000	1.492	2.028
3	0	0	0.21	0.33	0.33	300	85000	1.492	2.028
3	0	0	0.21	0.33	0.33	200	321000	1.492	2.028
3	0	0	0.21	0.33	0.33	180	793000	1.492	2.028
3	0	0	0.21	0.33	0.33	180	419000	1.492	2.028
3	0	0	0.21	0.33	0.33	350	56000	1.492	2.028
3	0	0	0.21	0.33	0.33	350	68000	1.492	2.028
3	0	0	0.21	0.33	0.33	160	10000000	1.492	2.028
3	0	0	0.21	0.33	0.33	400	39000	1.492	2.028
3	0	0	0.21	0.33	0.33	170	662000	1.492	2.028
3	0	0	0.21	0.33	0.33	160	9500000	1.492	2.028
3	0	0	0.21	0.33	0.33	400	46000	1.492	2.028
3	0	0	0.21	0.33	0.33	170	10000000	1.492	2.028
3	0	0	0.21	0.33	0.33	400	47000	1.492	2.028
3	0	0	0.21	0.33	0.33	170	452000	1.492	2.028

References

[1] Radaj D, Sonsino CM, Fricke W. Fatigue assessment of welded joints by local approaches. Cambridge: Woodhead Publishing Ltd; 2006.

[2] Niemi E, Fricke W, Maddox S. Fatigue analysis of welded joints – designer's guide to the structural hot-spot stress approach. Cambridge: Woodhead; 2006.

[3] Fricke W. IIW recommendations for the fatigue assessment of welded structures by notch stress analysis. Cambridge: Woodhead Publishing Ltd; 2012.

[4] Lazzarin P, Tovo R. A notch stress intensity factor approach to the stress analysis of welds. Fatigue Fract Eng Mater Struct 1998;1089–104.

[5] Lazzarin P, Zambardi R. A finite-volume-energy based approach to predict the static and fatigue behavior of components with sharp V-shaped notches. Int J Fract 2001;112(3):275–98.

[6] Haagensen PJ, Maddox SJ. IIW recommendations on post weld fatigue life improvement of steel and aluminium structures. Cambridge: Woodhead Publishing Ltd; 2013.

[7] Yildirim H, Marquis G. Fatigue strength improvement factors for high strength steel welded joints treated by high frequency mechanical impact. Int J Fatigue 2012;44:168–76.

[8] Marquis G, Mikkola E, Yildirim H, Barsoum Z. Fatigue strength improvement of steel structures by high-frequency mechanical impact: Proposed fatigue assessment guidelines. Weld World 2013;57(6):803–22.

[9] Yildirim H, Marquis G, Sonsino CM. Lightweight design with welded high-frequency mechanical impact (HFMI) treated high-strength steel joints from S700 under constant and variable amplitude loadings. Int J Fatigue 2016;91:466–74.

[10] Yildirim H, Marquis G, Barsoum Z. Fatigue assessment of high frequency mechanical impact (HFMI)-improved fillet welds by local approaches. Int J Fatigue 2013;52:57–67.

[11] Yildirim H, Marquis G. Fatigue design of axially-loaded high frequency mechanical impact treated welds by the effective notch stress method. Mater Des 2014;58:543–50.

[12] Yildirim H, Marquis G. Notch stress analyses of high-frequency mechanical impact-improved welds by using $\rho_f = 1mm$ and $\rho_f = \rho + 1$ approaches. Fatigue Fract Eng Mater Struct 2014;37(5):561–9.

[13] Yildirim H, Remes H, Nussbaumer A. Fatigue properties of as-welded and post-weld-treated high-strength steel joints: The influence of constant and variable amplitude loads. Int J Fatigue 2020;138.

[14] Marquis G, Barsoum Z. IIW collection IIW recommendations for the HFMI treatment for improving the fatigue strength of welded joints. Singapore: Springer Singapore; 2016.

[15] Hobbacher AF. IIW collection recommendations for fatigue design of welded joints and components. 2nd ed.. Singapore: Springer Singapore; 2016.

[16] Andrews R. The effect of misalignment on the fatigue strength of welded cruciform joints. Fatigue Fract Eng Mater Struct 1996;755–68.

[17] Iida K, Iino N. Fatigue strength of butt-welded joints angular distortion. In: Fracture mechanics of ductile and tough materials and its application to energy related structures. 1981, p. 293–302.

[18] Nguyen NT, Wahab M. The effect of undercut, misalignment and residual stresses on the fatigue behavior of butt welded joints. Fatigue Fract Eng Mater Struct 1996;19(6):769–78.

[19] Xing S, Dong P. An analytical SCF solution method for joint misalignments and application in fatigue test interpretation. Mar Struct 2016;143–161:50.

[20] Ahola A, Nykanen T, Bjork T. Effect of loading type on the fatigue strength of asymmetric and symmetric transverse non-load carrying attachments. Fatigue Fract Eng Mater Struct 2017;40(5):670–82.

[21] Ottersbock M, Leitner M, Stoschka M. Impact of angular distortion on the fatigue performance of high-strength steel T-joints in as-welded and HFMI condition. Metals 2018;8(5).

[22] Poutiainen I, Tanskanen P, Marquis G. Finite element methods for structural hot spot stress determination - a comparison of procedures. Int J Fatigue 2004;26:1147–57.

[23] Karakas O, Morgenstern C, Sonsino CM. Ffatigue design of welded joints from the wrought magnesium alloy AZ31 by the local stress concept with the fictitious notch radii of rf=1.0 and 0.05mm. Int J Fatigue 2008;30(12):2210–9.

[24] Gross R, Mendelson A. Plane elastostatic analysis of V-Notched plates. Int J Fract Mech 1972;267–76.

[25] Meneghetti G, Campagnolo A. Rapid estimation of notch stress intensity factors in 3D large-scale welded structures using the peak stress method. In: MATEC web conf. Vol. 165. 2018.

[26] Lazzarin P, Sonsino CM, Zambardi R. A notch stress intensity approach to assess the multiaxial fatigue strength of welded tube-to-flange joints subjected to combined loadings. Fatigue Fract Eng Mater Struct 2004;27(2):127–40.

[27] Lazzarin P, Livieri P, Berto F, Zappalorto M. Local strain energy density and fatigue strength of welded joints under uniaxial and multiaxial. Eng Fract Mech 2008;75:1875–89.

[28] Meneghetti G, Campagnolo A, Visentin A. Automated fatigue strength assessment of arc-welded structures according to the peak stress method. Procedia Struct Integr 2020;1062–83.

[29] Campagnolo A, Vormwald M, Shams E, Meneghetti G. Multiaxial fatigue assessment of tube-tube steel joints with weld ends using the peak stress method. Int J Fract 2020;135.

[30] Meneghetti G, Campagnolo A. State-of-the-art review of peak stress method for fatigue strength assessment of welded joints. Int J Fract 2020;139.

[31] Remes H. Strain-based approach to fatigue crack initiation and propagation in welded steel joints with arbitrary notch shape. Int J Fatigue 2013;52:114–23.

[32] Yildirim H, Marquis G. A round Robin study of high frequency mechanical impact treated welded joints subjected to variable amplitude loading. Weld World 2013;57(3):437–47.

[33] Ahola A, Bjork T. Fatigue strength of misaligned non-load-carrying cruciform joints made of ultra-high-strength steel. J Constr Steel Res 2020;175.

[34] Fricke W, IFricke W. IIW guideline for the assessment of weld root fatigue. Weld World 2013;57:753–91.

[35] Campagnolo A, Belluzzo F, Meneghetti G, Yildirim H. Fatigue strength assessment of as-welded and HFMI treated welded joints according to structural and local approaches. Int J Fatigue 2021.

[36] Shams-Hakimi Poja, Yıldırım Halid Can, Al-Emrani Mohammad. The thickness effect of welded details improved by high-frequency mechanical impact treatment. International Journal of Fatigue 2017;99:111–24. http://dx.doi.org/10.1016/j.ijfatigue.2017.02.023, https://www.sciencedirect.com/science/article/pii/S014211231730083X.

[37] Baumgartner J, Yildirim H, Barsoum Z. Fatigue strength assessment of TIG-dressed welded steel joints by local approaches. Int J Fatigue 126:72–8.
[38] Ottersbock M, Leitner M, Stoschka M, Maurer W. Analysis of fatigue notch effect due to axial misalignment for ultra high-strength steel butt joints. Weld World 2019;63(3):815–65.
[39] Nykanen T, Bjork Laitinen R. Fatigue strength prediction of ultra high strength steel butt-welded joints. Fatigue Fract Eng Mater Struct 2013;36(6):469–82.
[40] Jakubczak H, Glinka G. Fatigue analysis of manufacturing defects in weldments. Int J Fatigue 1986;51–7.
[41] Chiarelli M, Lanciotti A, Sacchi M. Fatigue resistance of MAG welded steel elements. Int J Fatigue 1999;1099–110.
[42] Remes H, Varsta P. Statistics of weld geometry for laser-hybrid welded joints and its application within notch stress approach. Weld World 2010;54.
[43] Burk BJ, Lawrence FV. Influence of bending stresses on fatigue crack propagation life in butt joint welds. Weld J 1977;56(2).
[44] Wylde JG, Maddox SJ. Effect of misalignment on fatigue strength of transverse butt welded joints. In: Proc. mech. eng. conference significance of deviations from design shape. 1979, p. 37–51.
[45] Gustafsson M. A study of thickness effect on fatigue in thin welded high strength steel joints. Steel Res Int 2006;77(12):873–81.